Clinical Science (2022) **136** 1281–1301
https://doi.org/10.1042/CS20220216

PORTLAND PRESS

Research Article

Multicellular regulation of miR-196a-5p and miR-425-5 from adipose stem cell-derived exosomes and cardiac repair

Nathalia C. de Almeida Oliveira[1,*], Elida A. Neri[1,*], Caio M. Silva[1,*], Iuri C. Valadão[1], Miriam H. Fonseca-Alaniz[1], Camila Zogbi[1], Débora Levy[2], Sergio P. Bydlowski[2] and Jose Eduardo Krieger[1]

[1]Laboratory of Genetics and Molecular Cardiology/LIM 13, Heart Institute (InCor), University of São Paulo Medical School, São Paulo, Brazil; [2]Lipids, Oxidation and Cell Biology Group/LIM 19, Heart Institute (InCor), University of São Paulo Medical School, São Paulo, Brazil

Correspondence: Jose Eduardo Krieger (j.krieger@hc.fm.usp.br)

Cardiac transplantation of adipose-derived stem cells (ASC) modulates the post-myocardial infarction (post-MI) repair response. Biomolecules secreted or shuttled within extracellular vesicles, such as exosomes, may participate in the concerted response. We investigated the exosome's microRNAs due to their capacity to fine-tune gene expression, potentially affecting the multicellular repair response. We profiled and quantified rat ASC-exosome miRNAs and used bioinformatics to select uncharacterized miRNAs down-regulated in post-MI related to cardiac repair. We selected and validated miR-196a-5p and miR-425-5p as candidates for the concerted response in neonatal cardiomyocytes, cardiac fibroblasts, endothelial cells, and macrophages using a high-content screening platform. Both miRNAs prevented cardiomyocyte ischemia-induced mitochondrial dysfunction and reactive oxygen species production, increased angiogenesis, and polarized macrophages toward the anti-inflammatory M2 immunophenotype. Moreover, miR-196a-5p reduced and reversed myofibroblast activation and decreased collagen expression. Our data provide evidence that the exosome-derived miR-196a-5p and miR-425-5p influence biological processes critical to the concerted multicellular repair response post-MI.

Introduction

Cardiac regeneration in response to injury is limited to a few hours or days after birth, as recently shown in mammalian models of myocardial infarction (MI) [1–4]. Shortly after birth and through adulthood, the repair is limited to collagen deposition and fibrotic tissue formation, primarily due to the lack of proliferative capacity in mature cardiomyocytes (CMs). While this response successfully prevents tissue rupture, it often results in progressive cardiac dysfunction and heart failure associated with increased morbidity and mortality [5–10].

Cell therapies, including transplantation of adipose-derived stem cells (ASC), can improve the post-myocardial infarction repair response [4,11–17]. We and others previously demonstrated that cardiac transplantation of ASC in animal models (rats and pigs) of myocardial infarction consistently stimulates angiogenesis, reduces inflammatory response, alters the characteristics of collagen fiber formation, and increases the relative amount of immature fibers within and around the infarction zone [4,18]. Despite these promising effects, ASC engraftment retention at injury sites is low and transient; it is believed that the benefits of ASCs are paracrine effects derived from biomolecules secreted or shuttled within extracellular vesicles like exosomes. These paracrine effects may involve cell communication strategies, including releasing cytokines, proteins associated with the matrix-cell perception of the microenvironment, and communication vesicles.

*These authors contributed equally to this work.

Received: 30 March 2022
Revised: 08 July 2022
Accepted: 26 July 2022

Accepted Manuscript online: 27 July 2022
Version of Record published: 05 September 2022

Clinical Science (2022) **136** 1281–1301
https://doi.org/10.1042/CS20220216

Exosomes are cell-derived vesicles with a diameter of 50–150 nm, thought to be involved in paracrine effects given their role in cell-to-cell communication. Studies demonstrate the effects of exosomes administration in mediating cardiac repair, improving cardiac functions, reducing CM apoptosis, promoting angiogenesis, and reducing fibrosis [19–21]. Nevertheless, the mechanisms by which exosomes promote these paracrine effects remain elusive [22].

MicroRNAs (miRNAs) in exosomes derived from mesenchymal stem cells (MSC) regulate processes associated with cardiac repair. For example, miR-199a, described by Eulalio et al. [23] and present within MSC-derived exosomes [24], is involved with CM proliferation and reduction of collagen deposition by cardiac fibroblasts (CFs) [25]. MiR-21, associated with apoptosis reduction in CMs and endothelial cells, when injected as enriched vesicles in a post-MI animal model, leads to improved cardiac function [26]. Although these studies underscore the importance of miRNAs in cardiac repair, most analyzed the effects of exosomal miRNAs in one or two cell types and lacked a thorough multicellular approach to test the concerted responses driven by these miRNAs.

To address these shortcomings and explore the regulatory roles of miRNAs derived from rat ASC-derived exosomes in post-MI cardiac repair, we profiled rASC-derived exosomes miRNAs and used bioinformatics to select the associated candidate miRNAs with multicellular responses. We focused on miR-196a-5p and miR-425-5p as candidate miRNAs with low expression levels in post-MI that might recapitulate vital characteristics of the effects of exosomes on cardiac repair. In the multicellular cardiac landscape, these miRNAs were associated with preventing CM mitochondrial dysfunction associated with ischemic conditions, increasing angiogenesis *in vitro*, polarizing macrophages to the M2 immunophenotype, and reducing and reversing fibroblast activation and collagen deposition.

Methods

Animal experiments

All experiments were carried out following the ethical principles in animal research of the Brazilian College of Animal Experimentation and were approved by the Institutional Animal Care and Use Committee of the University of São Paulo Medical School (Protocol 119/16). Wistar rats were purchased from the Institute of Biomedical Sciences, University of São Paulo, SP, Brazil. The rats were maintained in a temperature and humidity-controlled environment with a 12-h dark/light cycle at the Heart Institute (InCor) animal facility. Food and water were supplied *ad libitum*. Rats were euthanized with intraperitoneal injection of 50 mg/kg sodium thiopental (THIOPENTAX, Cristália, Brazil). Anesthetized rats were killed by cervical dislocation and inguinal adipose tissues and femur were collected.

Adipose tissue mesenchymal stem cells

We obtained rASCs from inguinal subcutaneous adipose tissue from 10-week-old Wistar rats. Cells were isolated, characterized, and maintained in culture as previously described [34,35]. Briefly, the adipose tissue was macerated, enzymatically dissociated, and centrifuged. The supernatants were discarded, and the pellets were resuspended in low-glucose Dulbecco's modified Eagle's medium (DMEM, Gibco, U.S.A.) supplemented with 10% (v/v) fetal bovine serum (FBS, cat. 12657029, lots 210320K and 210180K, Gibco, U.S.A.), 1% (v/v) sodium pyruvate (Gibco, U.S.A.), 100 IU/ml penicillin (Gibco, U.S.A.), and 100 μg/ml streptomycin (Gibco, U.S.A.) and plated at a density of 2.6×10^5/10 cm^2 in 100-mm plates (BD-Falcon, U.S.A.). Cells were cultured at 37°C with 5% CO_2. After 24 h, the non-adherent cells were discarded by changing the medium. Cell cultures were maintained until adherent cells reached 80–90% confluence with media being changed every 48 h. Then, rASCs were subjected to 0.05%-trypsin-EDTA (Gibco, U.S.A.) and re-plated at 1.0×10^4 cells/cm^2 (passage 1). Cultures were trypsinized every 7–10 days and used for experimental procedures at passage 3.

Isolation and analysis of exosomes

Exosomes were isolated from serum-free conditioned medium from rASCs (n=10) at passage three after 24-h conditioning. Supernatants from rASCs were passed through 0.22-μm filters to remove cell debris, and exosomes were purified by several centrifugation steps as previously described [28]. Briefly, supernatants were centrifuged at 2,000 $\times$ ***g*** at 4°C for 20 min to remove dead cells. The supernatants were ultracentrifuged at 100,000 $\times$ ***g*** at 4°C for 60 min, and exosome pellets were resuspended in 2 ml of PBS to wash and remove protein aggregates. An additional ultracentrifugation step at 100,000 $\times$ ***g*** at 4°C for 60 min was then performed (Ultracentrifuge, Beckman Coulter, L8-70M, U.S.A.). The pellets containing exosomes were resuspended in 200 μl of PBS or prepared for protein or RNA analysis. The protein content was measured using a BCA protein assay kit (Thermo Fisher Scientific, U.S.A.). We analyzed rASC-derived exosomes for the presence of the exosomal marker protein CD81 using flow cytometry as previously described [2]. Exosomal size and concentration were determined using NTA (Nanosight NS300, Malvern Instruments, U.K.). Using a 1-ml syringe, samples were injected slowly into the sample chamber, and the particles

were visualized using light scatter. Three movie recordings (20× magnification, 30 frames per second) were captured and then assessed to determine exosomes size and concentration.

Exosome labeling and uptake

For analysis of exosome uptake, exosomes were first stained with Dil Stain (Thermo Fisher Scientific, U.S.A.). After exosome isolation, the exosome pellet was resuspended in 1 μM Dil diluted in PBS and incubated at room temperature for 5 min. After ultracentrifugation (100,000 × ***g***, 1 h, 4°C), supernatants were discarded, and the exosome pellets were resuspended in PBS for a final exosome concentration of 50 μg/ml. Neonatal CMs and CFs cultured in CELLview glass-bottom slides (Greiner Bio-One, U.S.A.) were incubated with labeled exosomes for 3 h at 37°C with 5% CO_2. Cells were fixed in 4% paraformaldehyde for 10 min, washed with PBS, and stained with Alexa Fluor™ 488 Phalloidin (1:500; Thermo Fisher Scientific, U.S.A.) and DAPI (5 μg/ml, Thermo Fisher Scientific, U.S.A.) for 1 h at room temperature. Following washing with PBS, cells were imaged using confocal microscopy. Briefly, z-stacks (0.167 μm × 0.167 μm × 0.38 μm; xyz) were acquired on an Axio Observer.Z1 (Carl Zeiss, Germany) equipped with a Confocal Spinning Disk Unit (CSU-X1, Yokogawa, Japan) and a Rolera EM-C2 EMCCD camera (Teledyne Photometrics, U.S.A.). DAPI, phalloidin, and exosome staining were detected with sequential sample illumination at 405, 488, and 561 nm laser lines, respectively, using a C-Apochromat 40×/1.20 W Korr objective. Orthogonal views and 3D volume rendering of images were performed in Fiji [29,30] using "Orthogonal Views" and "3D Viewer" plugins, respectively.

Isolation and culture of neonatal CMs, CFs, and cardiac microvascular endothelial cells from rats

Neonatal CMs and CFs were isolated and cultured as previously described [31,32]. Heart samples from one-day-old Wistar rats were minced and digested with collagenase II (126 U/ml, Worthington, U.S.A.) and pancreatin (0.2 mg/ml, Sigma, U.S.A.) at 37°C six times with shaking for 15 min. Finally, cells were plated for 45 min (pre-plating) in plating medium [DMEM-Low and 199 media (4:1) containing 10% (v/v) horse serum (Gibco, cat 26050-088, lot 1517701, Origin: New Zealand), 5% (v/v) newborn calf serum (Gibco, cat 26010-074, lot 1418556, Origin: New Zealand), 100 U/ml penicillin plus 100 μg/ml streptomycin (Gibco, U.S.A.), and 1% bromodeoxyuridine (Sigma, U.S.A.)], which separated CMs (supernatant) and CFs (adhered cells). After incubation, the supernatants containing CMs were collected, and cells were counted manually. Adherent CFs remaining in the flask were cultured for 48 h in a medium containing high-glucose DMEM (Gibco, U.S.A.), 10% v/v FBS, 100 U/ml penicillin, and 100 μg/ml streptomycin.

For isolation of RCMVECs, an enrichment protocol was performed using a magnetic separation kit according to the manufacturer's instructions (Endothelial Cell Isolation Kit, rat, Miltenyi Biotec, U.S.A.). After the pre-plating process, supernatants were centrifuged, and cells were counted and subjected to a two-step procedure, first to remove non-endothelial cardiac cells and then select RCMVEC using specific markers. After separation, cells were resuspended in culture medium containing high-glucose DMEM 10% (v/v) FBS, 1% (v/v) sodium pyruvate, 1% (v/v) endothelial cell growth supplement (bovine hypothalamus, Thermo Fisher Scientific, U.S.A.), 1% (v/v) heparin sodium (5000 IU/ml, Blau Farmacêutica, Brazil), 100 IU/ml penicillin, and 100 mg/ml streptomycin and plated on plates previously treated with fibronectin (50 μg/ml, Sigma, U.S.A.) for at least 2 h. Cells were maintained in a humid atmosphere containing 5% CO_2 at 37°C.

MiRNA transfection of primary cell culture

The human miRNA mimics and inhibitors were obtained from Thermo Fisher Scientific. Sequences of all miRNAs and miRBase accession numbers are displayed in Supplementary Table S1. We transfected mimics, antagomirs and controls miRNAs into cells using a standard reverse transfection protocol at a final concentration of 40 nM. Briefly, target cells were seeded into 96-well fluorescence plates; 30 min later, we added transfection complex mix [Lipofectamine 2000 transfection reagent, (Thermo Fisher Scientific, U.S.A.) diluted in OPTI-MEM (Thermo Fisher Scientific, U.S.A.) combined with mirVana mimics miR-425-5p (ID: MC11575), miR196a-5p (ID: MC10068), and antagomirs miR-425-5p (ID: MH11575) and miR-196a-5p (ID: MH10068) (40 nM, Thermo Fisher Scientific, U.S.A.), prepared according to the manufacturer's protocol]. After transfection, each cell type was exposed to the appropriate treatment. Transfection efficiency was evaluated by flow cytometry with BLOCK-iT Fluorescent Oligo for lipid transfection (Thermo Fisher Scientific, U.S.A.) (Supplementary Figure S2A), and by RT-PCR of target genes of miRNA Mimic positive control and miRNA inhibitor. Thus, miR-1 Positive Control (cat 4464062, 40 nM, Thermo Fisher

Clinical Science (2022) **136** 1281–1301
https://doi.org/10.1042/CS20220216

Scientific, U.S.A.) reduced twinfilin-1 (*PTK9*) gene expression (Supplementary Figure S2B) and let-7c miRNA inhibitor positive control (cat 4464080, 40 nM, Thermo Fisher Scientific, U.S.A.) blocked endogenous let-7c miRNA and increased levels of *HMGA2* mRNA, as demonstrated by RT-PCR (Supplementary Figure S2C).

MirVana miRNA Mimic, Negative Control #1 (NTC) (cat 4464059; ThermoFisher Scientific, U.S.A.), BLOCK-iT Fluorescent and Control (Opti-MEM plus Lipofectamine) demonstrated the same level of $Ki67^+$ and EDU^+ in cardiomyocytes, fibroblast and endothelial cells (Supplementary Figure S2D). Opti-MEM plus Lipofectamine were using as a negative control in all experiments.

We used human miRNA mimics and antagomirs for transfection into rat and human cells.

Cardiomyocyte and non-myocyte hypoxia-induced proliferation

Cardiomyocytes were plated to confluence at 1×10^5 cells/cm^2 in 96-well fluorescence plates (Wells Greiner Microplate, Black, Clear Bottom, U.S.A.), previously treated with laminin for 2 h at 37°C. After 48 h in culture, cells were pre-treated with exosomes (50 μg/ml) or the same volume of PBS, and after 24 h. Plates were held for 24 h in 1% O_2, 94% N_2, and 5% CO_2 using a modular incubator (Model 3425, Thermo Fisher Scientific, U.S.A.). Cells cultured under a normoxic atmosphere served as the control.

For proliferation experiments, the cells were transfected as described above. After 48 h, the cell culture medium was replaced with a medium containing 5 mM EdU (Thermo Fisher Scientific, U.S.A.). Cells were cultured in hypoxic conditions for a further 24 h. Cells were fixed 72 h after plating with 4% Paraformaldehyde (PFA, Sigma, U.S.A.) at room temperature for 15 min and processed for immunofluorescence.

Measurements of lactate production under hypoxic conditions

Lactate production was measured using an ABL800 Flex blood gas analyzer (Radiometer, Denmark). The results were normalized by the number of cells in each treatment. Experiments were performed in triplicate.

Metabolic activity

According to the manufacturer's instructions, cell metabolic activity was evaluated using calcein-AM (Thermo Fisher Scientific, U.S.A.). Briefly, calcein-AM (10 μM) diluted in serum-free medium was added to cells and incubated for 60 minutes. After dye removal, cells were incubated for 15 min in a standard medium to allow AM ester removal. Live-cell imaging (37°C, 5% CO_2) was performed on the EVOS M7000 imaging system (Thermo Fisher Scientific, U.S.A.), and image analysis (mean calcein-AM fluorescence intensity per image) was performed using CellProfiler v.4.1.3.

ROS detection using CM-H_2DCFDA

CM-H_2DCFDA was used for oxidative stress detection. CMs plated in 96-well plates were incubated in 5 μM CM-H_2DCFDA (Thermo Fisher Scientific, U.S.A.) and 8.1 μM Hoechst (Thermo Fisher Scientific, U.S.A.) at 37°C for 30 min in a dark environment. After that, cells were washed with PBS, and images were acquired using an Evos M7000 microscope. CM-H_2DCFDA fluorescence intensity was analyzed at an excitation wavelength of 492–495 and an emission wavelength of 517–527 nm.

Mitochondrial dynamics and biosynthesis analysis

Cells were fixed in 4% paraformaldehyde for 10 min, then permeabilized with 0.1% Triton X-100 (Merck, U.S.A.) for 15 min. After washing in PBS, cells were incubated overnight with primary antibodies (TOM20, Mitofusin 1/2, DRP1, PGC1α, cTnT; Supplementary Table S2), and images were acquired using an Evos M7000 microscope. Approximately 4000 cells were imaged and segmented. Using Cell Profiler software, the cells had their inner particles (>3 pixels) counted and measured for mitochondrial attributes, including size and area. The aspect ratio (AR) was calculated as follows: $AR = M/m$, where M is the major axis length, and m is the minor axis length of a given structure. The major and minor axis lengths were obtained using the 'MeasureObjectSizeShape' module of CellProfiler software.

Cardiac fibroblast differentiation

Fibroblasts were plated at 1×10^5 cells/cm^2 in 96-well fluorescence plates (Wells Greiner Microplate, Black, Clear Bottom). At 24 h after plating, fibroblasts were subjected to a serum-free medium for 16 h and pre-treated with exosomes (50 μg/ml). After 24 h, cells were treated with TGF-β1 (R&D Systems, U.S.A.; 10 ng/ml) to induce fibroblast differentiation into myofibroblasts or TGF-β1 (Sigma, U.S.A.; 10 ng/ml) plus exosomes (50 μg/ml) for 48 h.

For the transfection experiments, the cells were transfected as described above. Twenty-four hours after transfection, the culture medium was replaced by a fresh medium containing TGF-β1 or PBS or exosomes, and cells were cultured for 48 h. Cells were fixed at 72 h after plating and processed for immunofluorescence.

Isolation of myofibroblasts cells from infarcted areas

Myofibroblasts from infarcted areas of adult rats were cultured to measure the effects of reversing the differentiation phenotype when subjected to various conditions using a protocol previously described [2]. Hearts were collected from adult rat hearts 15 days after descending artery ligation. Ventricles were placed into PBS, and only the injured fibrotic portion was digested. The ventricles were minced into small pieces to facilitate digestion and were placed into an enzyme solution of PBS containing 240 U/ml type 2 collagenase, 1 mg/ml trypsin, 1 mg/ml bovine serum albumin, and 10% penicillin/streptomycin. The tubes were incubated with shaking at 37°C for 15 min, and the supernatants were collected and transferred to conical tubes containing FBS. This process was repeated at least eight more times until the remaining pieces were too small to separate from the digestion solution. Cells were centrifuged at 400 × *g* for 5 min. The supernatants were discarded, and the pellets were resuspended in DMEM-high supplemented with 20% FBS and 1% penicillin/streptomycin. Resuspended cells were placed into a cell culture dish and incubated at 37°C in the presence of 5% CO_2. Experiments were performed in passage 4.

Bone marrow-derived macrophage (BMDMϕ) culture and polarization

As previously described, bone marrow from adult Wistar rats (300–350 g) was used for macrophage differentiation and polarization assays [2]. BMDMϕs were isolated from both hindlimbs and cultured to confluence at 6.5×10^5 cells/cm^2 in RPMI medium with 10% (v/v) FBS, 100 IU/ml penicillin, 100 μg/ml streptomycin, and M-CSF (400-28, Peprotech, U.S.A.; 30 ng/mL). After 7 days, BMDMϕs were seeded at 1.0×10^4 cells/well into 96-well clear bottom fluorescence plates accompanied with either the transfection complex mix containing Lipofectamine 2000 reagent with miRNA mimics (Thermo Fisher Scientific, U.S.A.; 40 nM) or 10 ng/ml IFN-γ (400-20, Peprotech, U.S.A.) for classical M1 polarization or 20 ng/ml IL-4 (400-04, Peprotech, U.S.A.) for M2 polarization or exosome (50 μg/ml). After polarization (48 h), cells were washed with PBS and fixed with 4% PFA at room temperature for 15 min for further staining.

Protein extraction and Western blotting

CMs were lysed in RIPA Lysis Buffer (Millipore, U.S.A.) containing protease and phosphatase inhibitors (Sigma, U.S.A.), and proteins were quantified using a BCA protein assay kit. Equivalent amounts of proteins were solubilized in sample buffer (0.5% SDS, 10% glycerol, 0.05% bromophenol blue, 50 mM dithiothreitol, 50 mM Tris, pH 6.8) and subjected to polyacrylamide gel electrophoresis in the presence of sodium dodecyl sulfate using polyacrylamide gels of various concentrations. After electrophoresis, proteins were transferred to polyvinylidene fluoride membranes (0.45, Amersham Hybond P, GE Healthcare, U.S.A.). Membranes containing the transferred proteins were incubated first in blocking solution (5% bovine serum albumin and 0.1% Tween 20 in TBS, pH 7.4) for 1 h at room temperature, followed by incubation for 16–18 h in specific primary antibody diluted in blocking solution at 4°C. The primary antibodies were anti-Bax (Cell Signaling Technology, U.S.A.) and anti-Bcl2 (Abcam, U.S.A.). The membranes were also incubated with primary antibodies specific for GAPDH (Abcam, U.S.A.) used as internal controls. After incubation for 1 h at room temperature with a secondary antibody conjugated to horseradish peroxidase (Thermo Fisher Scientific, U.S.A.), the bound primary antibody was detected using a chemiluminescent image analyzer (ImageQuant LAS 4000 mini, GE HealthCare, U.S.A.), and the images were quantified by densitometry using ImageJ software (Wayne Rasband, National Institute of Health, U.S.A.).

Immunofluorescence and high-content screening analyses

Cells were fixed in 4% paraformaldehyde for 10 min, then permeabilized with 0.1% Triton X-100 for 15 min. After washing in PBS, cells were incubated overnight with primary antibodies (Supplementary Table S2), washed with PBS, and incubated with appropriate conjugated secondary antibodies and DAPI (Supplementary Table S2) for 1 h at room temperature. Images were acquired using either the Image X Micro High-Content Platform (Molecular Devices, U.S.A.) or the Evos M7000. Multiwave Cell Scoring Metaexpress Software, Multiwave Cell Scoring, and CellProfiler v.4.1.3 [33] were used for data analysis. The sequential sets of image analysis modules for CellProfiler (i.e. pipelines) are available upon reasonable request.

Clinical Science (2022) **136** 1281–1301
https://doi.org/10.1042/CS20220216

Cell cycle

As previously described, the cell cycle was analyzed using propidium iodide (PI, Sigma, U.S.A.) [34]. First, the cell cycle was blocked using serum-free media for 24 h, and then cells were treated with exosomes (50 μg/ml) for 24 h. Finally, cells were harvested for cell cycle analysis. Cells were washed and fixed overnight in cold ethanol (70%). Fixed cells were washed and reconstituted in 250 μl of buffer (0.1% NP40, 0.2 mg/ml RNase, and 0.2 mg/ml PI) and incubated for 30 min at 4°C. Ten thousand events were collected from each sample using an Accuri BD flow cytometer (Becton Dickinson, U.S.A.), and the data obtained were analyzed using the FCS Express 4 program (De Novo Software, U.S.A.).

Endothelial proliferation and tube formation assay under normoxia

Human endothelial cells (HCAEC and HCMVEC; Lonza, U.S.A.) were cultured in an endothelial cell medium (EGM-2MV; Lonza, U.S.A.) for the proliferation assay and used in passages 4-6. Cells were plated to confluence at 0.7–1 $\times$ 10^4 cells/well in clear bottom 96-well fluorescence plates. Cells were cultured in a normoxic atmosphere and were treated with exosomes (50 μg/ml) or transfected as described above. After 48 h, the cell culture medium was replaced with a starvation medium containing 5 mM EdU. Cells were fixed 72 h after plating with 4% PFA at room temperature for 15 min and processed for immunofluorescence.

We used rat and human (HCMVEC) cardiac microvascular endothelial cells for the tube formation assay. Geltrex with low-dose growth factor (Thermo Fisher Scientific, U.S.A.) was added to 96-well plates for 30 min at 37°C for polymerization. RCMVEC were plated at 10 $\times$ 10^3 cells per well and incubated with exosomes (50 μg/ml) or VEGF (50 μg/ml, R&D, U.S.A.) at 37°C. HCMVEC were transfected as described above; after 48 h, they were plated at 10 $\times$ 10^3 cells per well in 96-well plates with Geltrex and incubated with exosomes (50 μg/ml). Six hours later, network structures were photographed with an inverted microscope using a 4× objective, and the total length of the tube was quantified using ImageJ software (Wayne Rasband, National Institute of Health, U.S.A.) and the Angiogenesis Analyzer plugin. Representative segmentation results are shown in Supplementary Figure S6.

Real-time polymerase chain reaction (RT-PCR)

Total RNA was extracted from CF using TRIzol reagent (Thermo Fisher Scientific, U.S.A.) following the manufacturer's instructions. After total RNA extraction, 5 μg of RNA were reversely transcribed into cDNA using the SuperScript III first-strand synthesis system for RT-PCR kit (Thermo Fisher Scientific, U.S.A.) in a T100 Thermal Cycler (BioRad, U.S.A.). Quantitative determination of mRNA levels was performed using a QuantStudioTM 12k Flex Real-Time PCR System (MicroAmp Optical 384-Well Reaction Plate, U.S.A.) under the following conditions: initial denaturation at 95°C for 10 min; 40 cycles of denaturation at 95°C for 15 s, annealing and extension at 60°C for 1 min; final extension at 72°C for 5 min. The fluorescent signal was measured at the end of every cycle. Expression levels were estimated in triplicate, and B2M and GAPDH were used as normalizers. The determination of fold-expression was calculated using the DDCt method according to Livak and Schmittgen [35]. Primer sequences are displayed in Supplementary Table S3.

Exosomal miRNA extraction and microarray

Total RNA was extracted from rASC-derived exosomes ($n = 6$ animals) using TRIzol reagent and purified miRNA was obtained using miRNeasy (QIAGEN, U.S.A.) following the manufacturer's instructions. We labeled 130 ng of miRNA using a FlashTag Biotin HSR RNA Labeling Kit (ThermoFisher Scientific, U.S.A.). The biotinylated miRNA was then hybridized to GeneChipTM miRNA 4.1 array plates (Thermo Fisher Scientific, U.S.A.), washed, and stained according to the manufacturer's protocols. The miRNA array plates were scanned using a GeneTitanTM Instrument. Expression Console Software was used to create summarized expression values (CHP-files). A robust multichip analysis algorithm was applied. Data were analyzed using Transcriptome Analysis Console software.

MiRNA pathway enrichment and network analysis

Target genes of miRNAs were selected through the multiMiR package [36] using the database options with validated or predicted information. The databases consulted to receive the putative target genes of miRNAs were miRanda, miRdb, microcosm, and Elmmo.

For the construction of the interaction networks between genes and miRNAs, the iGraph package of R was used [37]. The network nodes included the miRNAs and genes, edges were their predicted interactions, and the degree of interaction was the size of the nodes. We selected interactions with degrees more significant than two in the network, and the Fruchterman-Reingold direct-force visualization layout was used.

Gene ontology analyzes were performed using the clusterProfiler package [38]. For enrichment analysis, we selected only pathways with more than five enriched genes and with adjusted *P*-values lower than 0.05. To select the miRNAs present in humans and with validated interactions, the DIANA-miRPath tool was used (Tarbase V7.0). Then, a heatmap that demonstrates pathways enriched in miRNAs was generated using the pathway union function with all target genes present in the microT-CDS database.

To better understand the profile of pathways modulated by miR-196a-5p and miR-425-5p, gene ontology and enrichment analyses were performed. The mirDB database was used to determine possible target genes for this miRNA. The selection of pathways most represented by predicted genes and miRNA targets was performed using the online tool for functional annotation DAVID [39]. The selected pathways contained more than two genes and with an adjusted *P*-value < 0.05.

MI gene expression database integration

The data provided by the authors of normalized quantile expression from the GSE81636 and GSE36239 datasets were obtained. To integrate each post-infarction moment (2D, 14D, 28D), the data were normalized concerning the overall mean expression of all genes in the samples of their respective control and transformed into log2. Only miRs in common at the three post-infarction time points were represented in the heatmaps.

Statistical analyses

Statistical analyses and graphical representations were performed using GraphPad Prism software (GraphPad Softwares Inc.). Two-group analyses were performed using the paired Student's *t* test. One-way analysis of variance and the Tukey test were used for more than two groups. Statistical significance was determined as $P<0.05$.

Results

Characterization of r-ASC-derived exosomes and target cell uptake

Exosomes were isolated from serum-free conditioned media of rASCs. Cells exhibited the typical antigen expression profile of $CD73^+$ $CD90^+$ $CD29^+$ $CD45^-$ $CD31^-$ (Supplementary Figure S1A). Flow cytometry confirmed the presence of specific exosome marker CD81 (Supplementary Figure S1B) in rASC-derived exosomes. We determined the size of exosomes (Supplementary Figure S1C) and the hydrodynamic diameter of exosomes (∼117 nm, ranging from 50 to 200 nm) using nanoparticle tracking analysis (NTA) (Supplementary Figure S1D). Using confocal microscopy, we confirmed the internalization of rASC-derived exosomes by CFs (Supplementary Figure S1E, S1G) and neonatal CMs (Supplementary Figure S1F, S1H).

Effects of rASC-derived exosomes on cardiac target cells and macrophages

We exposed neonatal CMs and non-myocytes to exosomes (50 μg/ml) for 24 h under normoxia and hypoxic (1% O_2) conditions. Under hypoxia, exosome-treated neonatal CM showed a ∼25% higher proliferation rate than phosphate-buffered saline (PBS)-treated cells (Figure 1A), whereas we observed a ∼27% decreased proliferation in exosome-treated tropomyosin-negative non-myocytes, as indicated by incorporation of Ki-67 (Figure 1B). Under normoxia conditions, the pattern was less pronounced. We observed no differences in CM proliferation after 24 or 48 h exposure to exosomes (Supplementary Figure S4A and S4B), and non-myocytes proliferated ∼14% less in response to exosome influence (Supplementary Figure S3C).

We observed a ∼5% enhanced proliferation of rat cardiac microvascular endothelial cells (RCMVECs) (Figure 1C) and increased tube formation in a Matrigel assay, consistent with enhanced angiogenic capacity (Figure 1D) in response to exosomes.

Next, we evaluated the effect of the exosomes on rat bone-marrow-derived macrophage polarization and activation. We compared the response to the control macrophage cells M0 (without stimulus), M1 polarized cells (IFNγ), and M2 cells (IL-4). We observed that exosome exposure increased the expression of IL-1β, TNF-α, arginase-1, and CCL2 in macrophages, with no immunophenotype specificity (Figure 1E).

To test the notion that exosomal capacity to prevent TGF-β1 (10 ng/ml) activation of CFs into myofibroblasts, we pre-treated CF with exosomes (50 μg/ml) for 24 h before TGF-β1 stimulation. Exosomes significantly prevented TGF-β1-induced α-SMA protein (Figure 1F) and gene (Figure 1G) expression. Pre-treatment with exosomes abrogated the TGF-β1-induced increase in collagen I mRNA expression (Figure 1G).

Clinical Science (2022) **136** 1281–1301
https://doi.org/10.1042/CS20220216

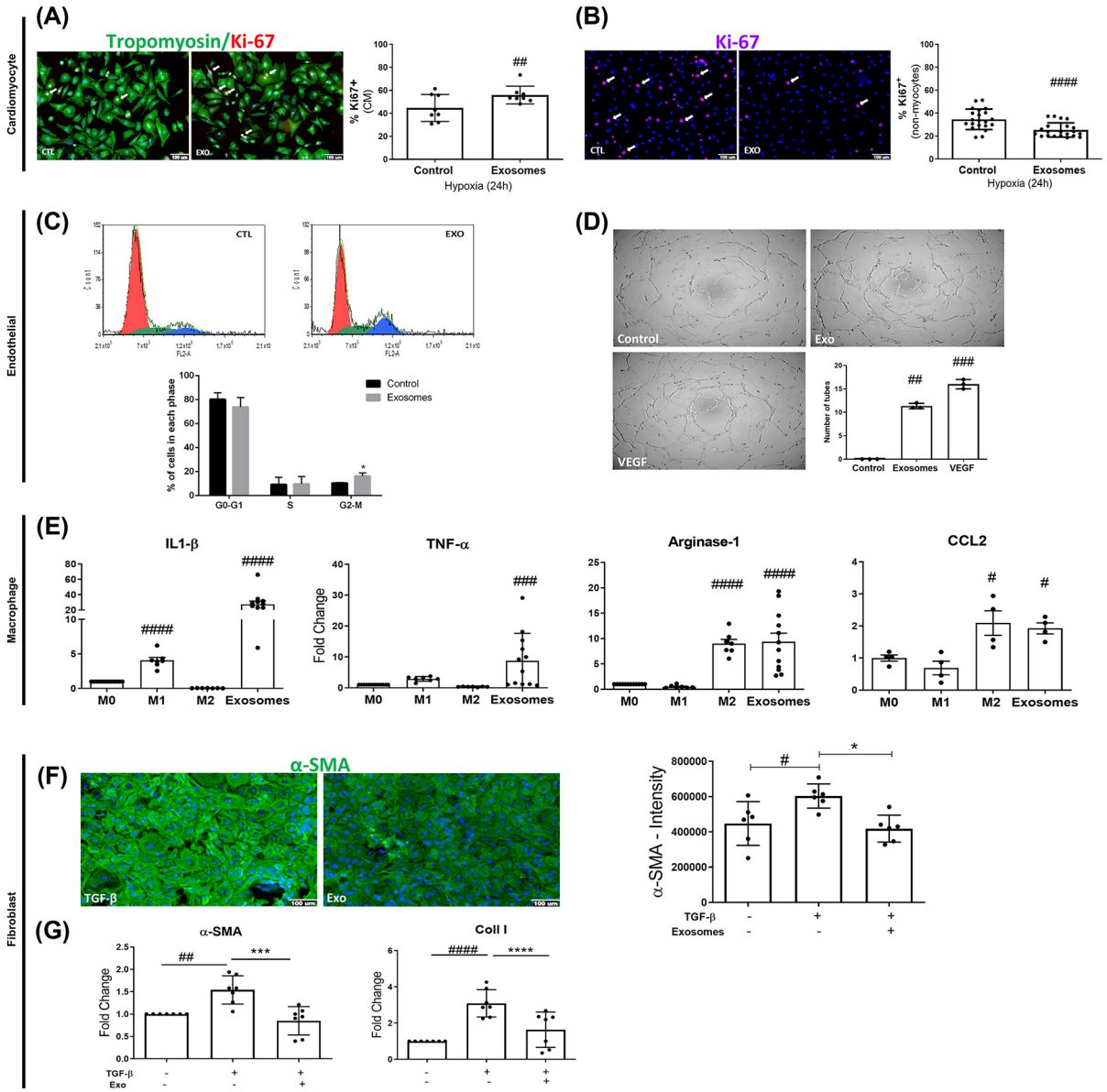

Figure 1. RASC-derived exosomes modulate proliferation, tube formation, and macrophage and fibroblast activation

Representative images and quantification of Ki67$^+$ CMs (**A**) and non-myocytes (**B**) on control and exosome-treated mixed culture submitted to hypoxia. (**C**) Flow cytometry histograms of DNA quantification by DAPI in control and exosome-treated cells. Red, green, and blue areas represent the counting of cells in the cell cycle's G0-G1, S, and G2-M phases. The bar graph represents the percentage of cells classified into each of these three phases. (**D**) Representative bright-field images of tube formation assay in Matrigel; magnification: 4×. The bar graph represents the number of tubes formed by control, exosome, and VEGF-treated cells (positive control). (**E**) Bar graphs representing expression levels of M1 gene markers (IL-1β, TNF-α) and M2 markers (arginase-1 and CCL2) in unstimulated macrophages (M0), IFN-γ- (M1), IL-4- (M2), and exosome-treated. Expression level is relative to control (M0). (**F**) Representative micrographs and quantification of α-SMA mean fluorescence intensity in control fibroblasts treated with TGF-β only or TGF-β plus exosomes. (**G**) Bar graphs representing gene (left) and protein (right) expression levels of α-SMA and Coll I, respectively, relative to control. Graphs are presented as mean ± SD. Statistical analysis was performed using the *T*-test (A,B) or one-way analysis of variance followed by the Tukey test for multiple comparisons (**C–G**). All experiments were repeated independently at least four times. # and * symbols represent statistically significant differences relative to control and TGF-β-treated cells, respectively. * and $^{\#}P<0.05$, ** and $^{\#\#}P<0.01$, *** and $^{\#\#\#}P<0.001$, **** and $^{\#\#\#\#}P<0.0001$.

These results suggest that rASC-derived exosomes modulate the cardiac repair response in multiple cell targets by promoting neonatal CM and endothelial cell proliferation and angiogenesis, inducing macrophage inflammatory and alternative polarization immunophenotype, and preventing CF activation and increased collagen I expression.

RASC-derived exosomes contain enriched miRNAs with the potential to modulate cardiac repair in multicellular targets

Exosomes contain molecules that individually (or in combination) modulate complex processes such as cardiac repair. Recently, miRNAs have been proposed as candidate effectors during cardiac remodeling. We used a microarray platform (728 mature rat miRNAs, array GeneChip™ miRNA 4.1, Thermo Fisher Scientific) to determine the miRNAs landscape of rASC-derived exosomes. We considered only miRNAs detected in all samples and a minimum raw expression signal of $\log_2 > 4.0$ for further analysis. We found 116 miRNAs derived from rASC-derived exosomes (Supplementary Table S4) and focused on rASC-derived exosomes miRNAs not yet tested for cardiac repair (Figure 2A). We selected 35 miRNAs with no validated interactions with genes in databases such as miRecords and MiRTarBase for our subsequent exploratory analyses. According to four databases, these 35 miRNAs were predicted to make 6322 gene–miRNA interactions. We filtered from this set of miRNAs the under-represented (<10 genes) and over-represented (>500 genes) interactions, leaving 27 miRNAs. The expression levels of these 27 miRNAs are depicted in Figure 2B. By analyzing the topological characteristics of the miR-gene interaction networks, we filtered interactions with a degree lower than two (Supplementary Figure S3A). Using the set of persistent genes, we performed a gene ontology analysis that revealed over-represented pathways, including 'response to hypoxia,' 'Regulation of cytoskeleton organization,' and 'Response to extracellular stimuli' that may be related to cardiac repair and multicellular effects (Supplementary Figure S3B and S3C). We found 25 miRNAs involved with these three GOs that demonstrate a high degree of connectivity (Figure 2C). We then narrowed the analysis to the miRNAs with human homologs, validated interactions in databases, and expressed in myocardial infarction (Supplementary Figure S3D and S3E). We integrated information available using the DIANA-miRPath tool (v.3) and expression data from two different works available on the Gene Expression Omnibus platform that represent different post-MI days (i.e., 2, 14, and 28 days) (Figure 2D).

Based on the previous analysis, we identified five miRNAs with the potential to be associated with biological processes affecting cardiac repair (Figure 2D). After performing an extensive literature search, we selected miR-196a-5p and miR-425-5p, both of which had not been studied previously in cardiac repair. We identified the predicted target genes of these two miRNAs in the miRDB and TargetScan databases and investigated the primary pathways enriched by these genes. For miR-196a-5p, we found enriched pathways favoring multicellular processes, including cell proliferation, collagen synthesis, inflammatory response, endothelial barrier, and mitochondrial control (Figure 2E). The miR-425-5p-enriched pathways were related to energy control cascades, CM stimuli, and down-regulation of apoptosis (Figure 2F).

RASC-derived exosomal miR-196a-5p and miR-425-5p do not affect cell proliferation and viability of CMs under hypoxic conditions

Our next objective was to determine the effect of the miR-196a-5p and miR-425-5p overexpression on the proliferative potential of CMs upon hypoxia exposure. To assess functional cellular effects, overexpression was selected based on the low expression levels of both miRNAs in the context of infarction, as shown in Supplementary Figure S3E. We performed reverse transfection of isolated neonatal rat ventricular CMs with both miRNAs. In a 1% O_2 environment, the levels of proliferative CMs (α-actinin$^+$ 5-ethynyl-29-deoxyuridine [EdU]$^+$) and non-myocytes (α-actinin$^-$EdU$^+$) were evaluated using immunofluorescence. Hypoxia was confirmed by increased lactate production, which was partially attenuated by miR-425-5p and miR-196a-5p mimics (Figure 3A). The proliferation of CMs was enhanced only by exosomes (Figure 3B and Supplementary Figure S4E), whereas exosomes and both miRNAs mimics inhibited the proliferation of non-myocytes cells (Figure 3C). Under normoxia, exosomes did not affect CM and fibroblasts proliferation after 24 and 48 h of treatment even with a higher exosome concentration (Supplementary Figure S4A–D).

Because hypoxia and exosome/miRNA treatments may influence cell metabolism, we determined whether treated CMs increased metabolism, reactive oxygen species (ROS) levels, and apoptosis rate. We assessed mitochondrial integrity by evaluating calcein-AM fluorescence levels and detected increased levels on exosomes and microRNAs 425-5p and 196a-5p mimics' treatments. Inhibition of miR-425-5p and 196a-5p resulted in no differences compared with control. These data are consistent with an increased metabolic activity in response to exosome and miR-mimics exposure on (Figure 3D). In contrast, ROS levels decreased in cells treated with exosomes or miRNAs under hypoxia (Figure 3E). MiR-425-5p antagomir was less efficient in preventing ROS production by ∼28% compared with its

Clinical Science (2022) **136** 1281–1301
https://doi.org/10.1042/CS20220216

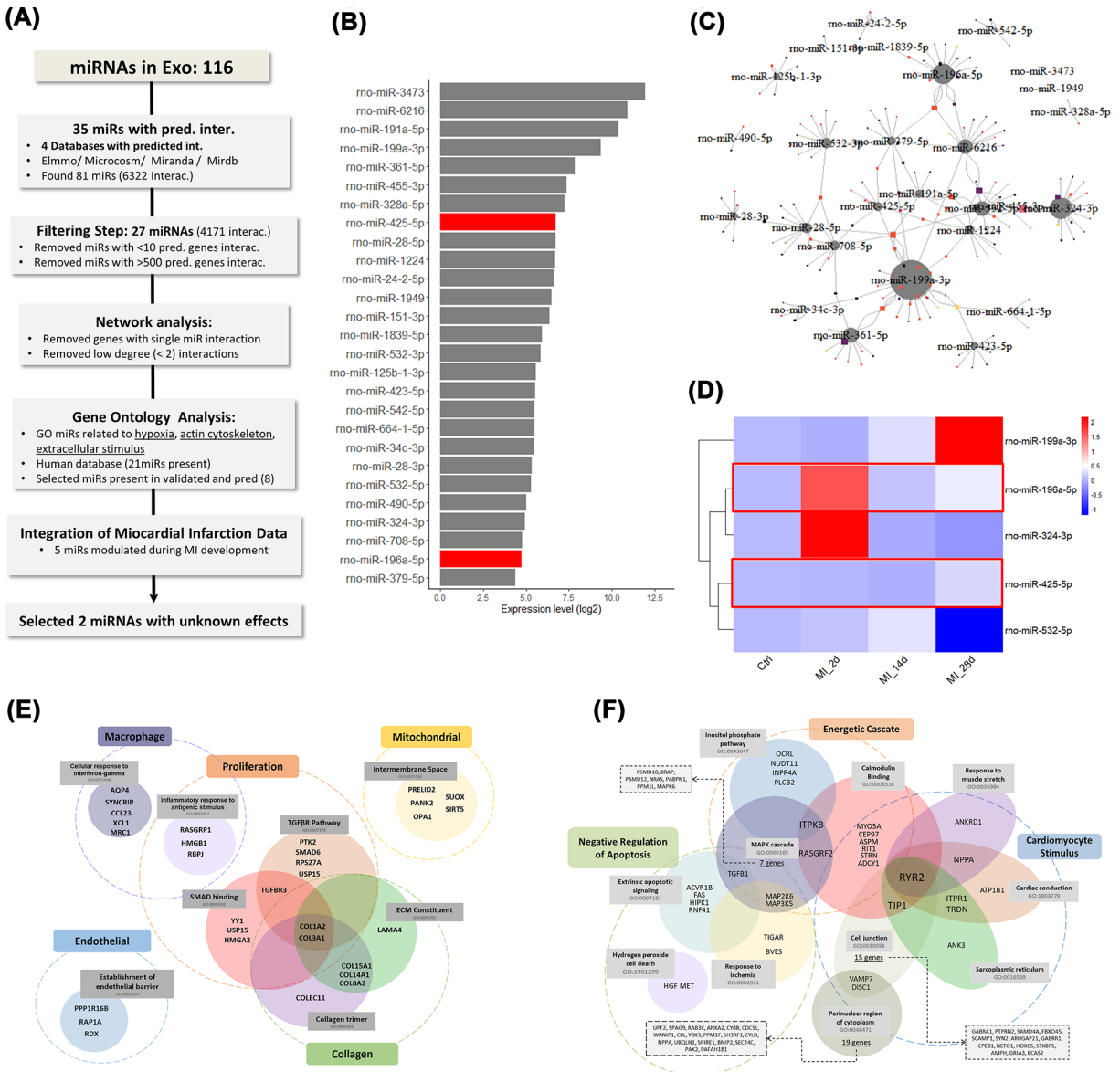

Figure 2. Analysis pipeline for selecting exosomal miRNAs released by ASCs and associated with multicellular effects and cardiac repair response

(**A**) Representative scheme of the analysis and filtering steps performed to select the analyzed miRNAs. (**B**) The expression level of 27 exosomal miRNAs remaining after database analysis and filtering. (**C**) Network of interactions of selected miRNAs with a degree of interaction greater than two. MiRNAs are represented by gray circles and genes by colored squares. The sizes of the gray circles represent the degree of interaction of miRNAs with their putative target genes. (**D**) Heatmap represents the five miRNAs' expression levels associated with multicellular processes and cardiac repair. The figure shows the integration of the databases containing the different days of myocardial infarction. The red bars around miR-196a-5p and miR-425-5p represent the miRNAs selected for subsequent analyses, given the lack of characterization of their effects on cardiac repair. Diagram of ontological pathways enriched for miR-196a-5p (**E**) and miR-425-5p (**F**) associated with multicellular processes. The filled circles show the names and codes of the enriched pathways, the enriched genes targeted by the selected miRNAs, and the overlaps with other pathways. Dotted circles demonstrate broad associations with cellular effects and functions. The data are represented as mean ± SEM of six independent experiments with cells obtained from different rats.

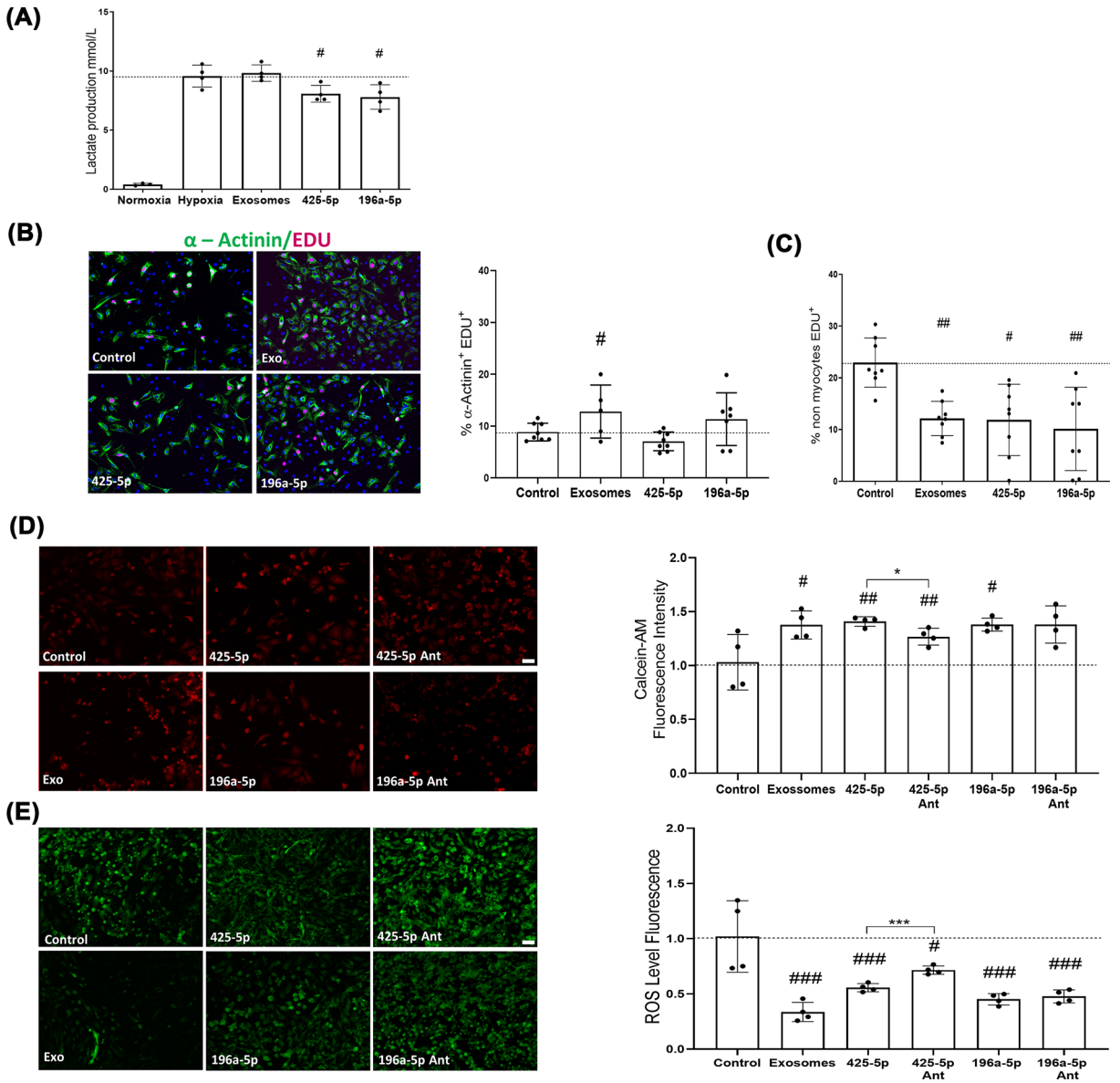

Figure 3. miR-196a-5p and miR-425-5p improve the viability of hypoxic CMs without altering proliferation

Mixed cultures of CM and non-myocytes were treated with exosomes or transfected with miR-425-5p and miR-196a-5p before being subjected to analysis of lactate production, proliferation, apoptosis, and cell metabolic viability. (**A**) The bar graph represents lactate production (mmol/L) by rat neonatal CMs under normoxia or treated with exosomes, miR425-5p, and miR196a-5p under hypoxia. Representative micrographs and proliferative CMs (**B**) and non-myocytes (**C**) quantification in mixed culture after treatment with exosomes, miR-425-5p and miR196a-5p. Representative micrographs and calcein-AM (**D**) and ROS quantify mean fluorescence intensity (**E**) in mixed cultures treated with exosomes, miR-425-5p and miR-196a-5p mimics and antagomirs. Graphs are presented as mean ± standard deviation. All experiments were repeated independently at least four times. Statistical analysis was performed using a one-way analysis of variance followed by the Tukey test for multiple comparisons. $^{\#}P<0.05$, $^{\#\#}P<0.01$ and $^{\#\#\#}P<0.001$, relative to the control group.

mimic while miR-196a-5p and its antagormir showed no difference. Treatment of CM-enriched cell cultures with exosomes and microRNAs did not alter the Bax/Bcl2 protein expression ratio, consistent with increased cell preservation (Supplementary Figures S5A–D and S6).

These results suggest that miR-196a-5p and miR-425-5p decrease ROS levels and do not modify CM proliferation or viability under hypoxic conditions, whereas they decrease the proliferation of non-myocytes.

Clinical Science (2022) **136** 1281–1301
https://doi.org/10.1042/CS20220216

RASC-derived exosomal miR-196a-5p and miR-425-5p affect mitochondria dynamics and biogenesis in CMs

Because mitochondrial dynamics are altered under hypoxia [27], and mitochondrial health status might be associated with improved cardiac repair, we measured the amount and size of mitochondria in exosome- and miRNA-treated CMs.

Mitochondria number and morphology of exosome- and miRNA-treated CMs were evaluated using TOM20 staining in cardiac troponin T-positive cells (cTnT) (Figure 4A). Mitochondria number, area and aspect ratio (i.e., the ratio between mitochondria major and minor axes) were increased by exosome treatments. MiR-425-5p overexpression increased area and aspect ratio, whereas miR-425-5p inhibition reversed the area increase but did not influence the aspect ratio. MiR-196a-5p mimic increased the number of mitochondria, whereas the antagomir reversed this response (Figure 4A).

We next measured mitochondria fission, fusion, and biogenesis in response to exosomes and miRNAs mimics. Exosomes and all microRNAs treatments up-regulated the fusion protein mitofusin1/2 compared with control (Figure 4B) without modulating the protein DRP1, a regulator of the fission process (Supplementary Figure S7A). Overexpression or inhibition of miR-425-5p increased mitofusin1/2 protein levels. Inhibition of miR-196a-5p increased mitofusion1/2 amount in ∼8% compared with overexpression (Figure 4B). Exosomes decreased the levels of the mitochondria biogenesis-associated protein PGC1α (Figure 4C). These findings suggest that mitochondria-related alterations are differentially affected by exosomes and miRNAs. Improvements in mitochondria fusion and biogenesis are consistent with beneficial modulation of cardiac repair.

RASC-derived exosomal miR-196a-5p and miR-425-5p promote proliferation and tube formation of human endothelial cells

We then determined whether the miRNAs modulate the endothelial cells proliferation rate *in vitro*, and found that exosomes and miR-196a-5p mimic increased the percentage of EdU^+ incorporation in Human Coronary Artery Endothelial Cells (HCAEC). In contrast, the antagomir did not affect cell proliferation (Figure 5A). Interestingly, on a second primary culture of human endothelial cells, human microvascular endothelial cells (HMVEC), only miR-196a-5p mimic increased the number of EdU^+ (Figure 5B) and $Ki67^+$ (Figure S8B) while exosomes and miR-196a-5p inhibition showed no effect (Figure 5B).

To test whether the miRNAs functionally modulate endothelial cells' angiogenic capacity, we evaluated miRNA-treated human cardiac microvascular endothelial cells (HCMVECs) in reconstituted basement membrane matrix (Matrigel) and observed that exosomes and miR-196a-5p and miR-425-5p mimics increased tube formation (Figure 5C and Supplementary Figure S8A). These findings suggest that the miRNAs recapitulate the exosomal effects on endothelial cells and the responses are vascular bed-specific.

RASC-derived exosomal miR-196a-5p and miR-425-5p modulate macrophage polarization

We evaluated the expression of markers of phenotype polarization using real-time RT-PCR in non-polarized macrophages exposed to exosomes and miRNAs for 48 h. As controls, we used cells exposed to LPS+/gamma interferon (IFN-γ) and IL-4, which direct the macrophages toward M1 and M2 immunophenotypes, respectively (Figure 6A).

Specific gene markers for the M1 profile (*IL-1*β and *TNF-*α expression levels) were increased only by the exposure to exosomes (Figure 6A,B), whereas the reparative M2 profile markers (*arginase-1* and *CCL2*) were increased in response to both exosomes and miRNAs mimics (Figure 6C,D). The miRNA-425-5p antagomir induced both M1 and M2 gene expressions, an effect similar to exosomes (Figure 6A–D). Interestingly, miR-196a-5p antagomir did not regulate M1 (Figure 6A,B) or M2 (Figure 6C,D) markers expression, demonstrating an opposite effect of its mimic relative to M2 polarization.

These findings suggest that the selected miRNAs drive macrophages to a unique immunophenotype, whereas exosomes have broader immunomodulatory effects. The data also suggest that these miRNAs induce macrophage shifting toward the M2 profile, consistent with the notion of diminishing the inflammatory process and activation of repair pathways.

Clinical Science (2022) **136** 1281–1301
https://doi.org/10.1042/CS20220216

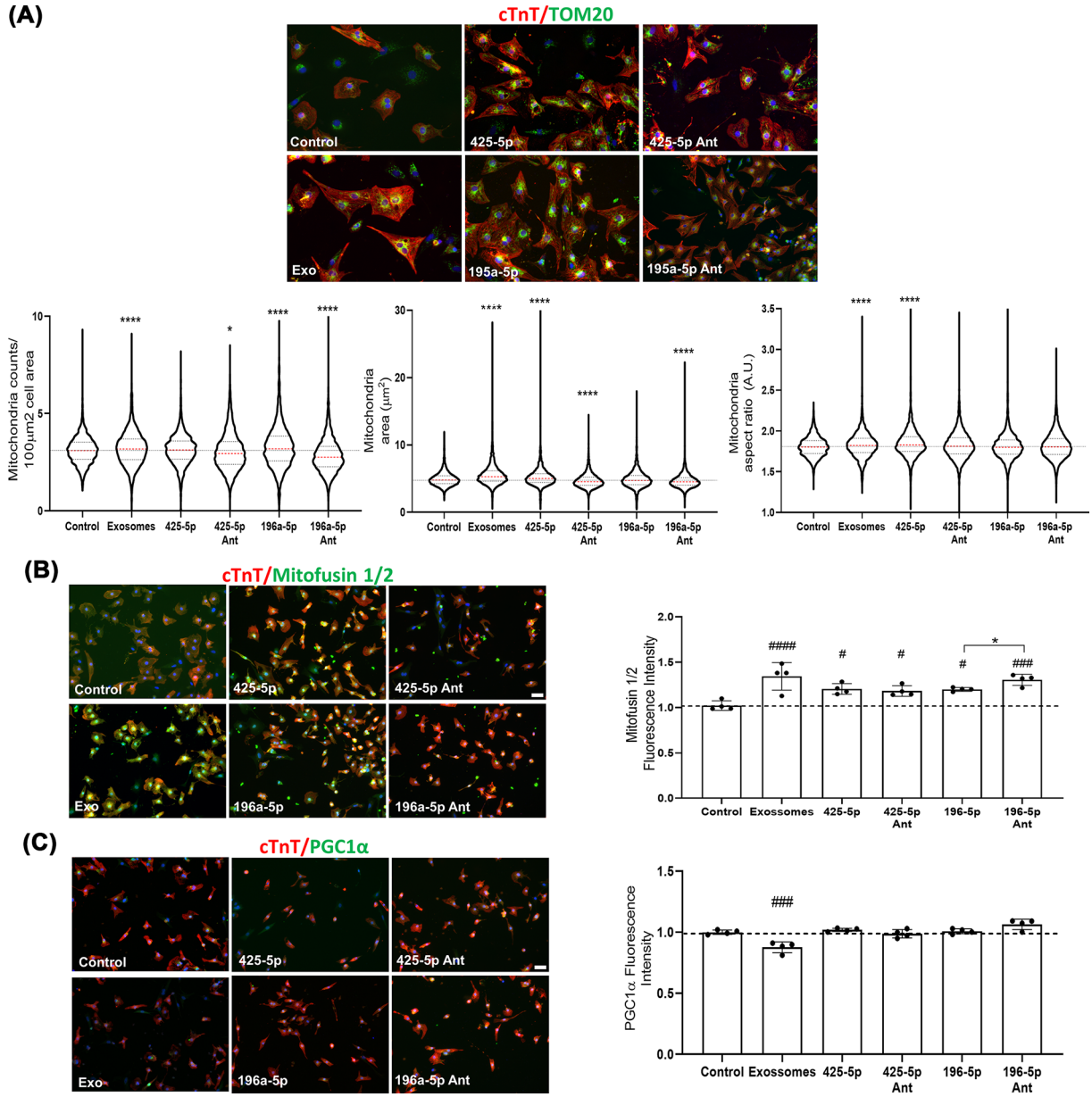

Figure 4. miR-196a-5p and miR-425-5p differentially induce mitochondrial fusion in CMs

Mixed cultures of CM and non-myocytes were treated with exosomes or transfected with miR-425-5p and miR-196a-5p before immunofluorescence-based analysis of mitochondria morphology and related markers. (**A**, left) Representative immunofluorescence of cTnT and TOM20 in a mixed culture of rat neonatal CMs and non-myocytes. (**A**, right) Violin plots represent mitochondria density, area, and aspect ratio in cTnT$^+$ cells. Representative micrographs and quantification of mitofusin1/2 (**B**) and PGC1α (**C**) mean fluorescence intensity in cTnT$^+$ cells of mixed cultures treated with exosomes, miR425-5p and miR-196a-5p mimics and antagomirs. Graphs are presented as mean $\pm$ standard deviation. All experiments were repeated independently at least four times. Statistical analysis was performed using a one-way analysis of variance followed by the Tukey test for multiple comparisons. * and $^{\#}P<0.05$, ** and $^{\#\#}P<0.01$, *** and $^{\#\#\#}P<0.001$, **** and $^{\#\#\#\#}P<0.0001$.

The effects of rASC-derived exosomal miR-196a-5p and miR-425-5p on CF activation

We used a preventive model of fibroblast activation in which we pre-exposed the cells to exosomes or miRNAs for 24 h followed by treatment with TGF-β1 for 48 h (Figure 7A) to assess the effects of the miRNA, and we also used a therapeutic model to reverse the activated fibroblasts previously exposed to TGF-β1 for 24 h (Figure 7B).

Clinical Science (2022) **136** 1281–1301
https://doi.org/10.1042/CS20220216

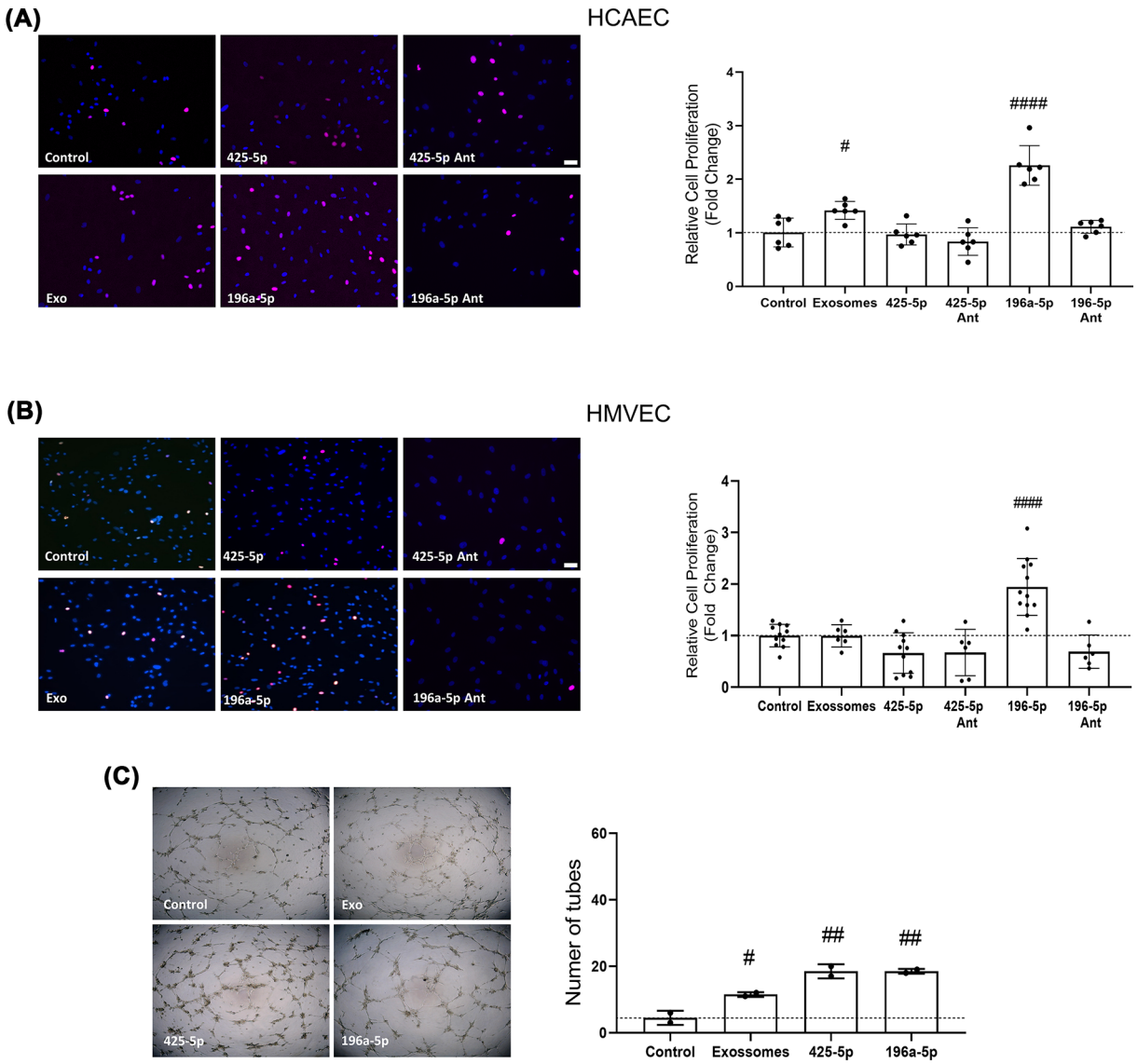

Figure 5. miR-196a-5p and miR-425-5p cause angiogenic response in endothelial cells

Proliferative and tubule formation potential of HCAEC and HMVEC treated with exosomes, miR-425-5p and miR-196a-5p mimics and antagomirs were evaluated by EdU incorporation and tube formation assay in Matrigel, respectively. (**A**) Representative micrograph and quantification of EdU incorporation in control and treated HCAEC (A) and HMVEC (**B**). All experiments were repeated independently at least four times. (**C**) Representative bright-field micrographs (magnification: 4×) and quantification of tube formation by exosome and miRNA-treated cells, data are presented as mean ± SD, n=2 repeated independently. Graphs are presented as mean ± standard deviation. Statistical analysis was performed using a one-way analysis of variance followed by the Tukey test for multiple comparisons. $^{\#}P<0.05$, $^{\#\#}P<0.01$, $^{\#\#\#}P<0.001$ and $^{\#\#\#\#}P<0.0001$, relative to the control group.

We used fluorescence microscopy to examine the effects of exosomes, miR-196a-5p (mimic and anatagomir) or miR-425-5p on targeted processes.

We found that exosomes and miR-196a-5p mimic prevented and reversed the TGF-β1-induced increase of α-SMA (Figure 7C,D) and Col I (Figure 7E,F), whereas miR-425-5p mimic did not affect these phenotypes. Inhibition of miR-196-5p did not affect α-SMA (Figure 7C) and Col I (Figure 7E) expression in cardiac fibroblasts. Preliminary data indicated that overexpression or inhibition of miR-425-5p did not influence these phenotypes in cardiac fibroblasts (data not shown).

Next, we evaluated whether these interventions reduced profibrotic signaling in differentiated myofibroblasts isolated from infarcted hearts of adult rats. The exosomes and miR-196a-5p mimic reduced levels of α-SMA and Col I in

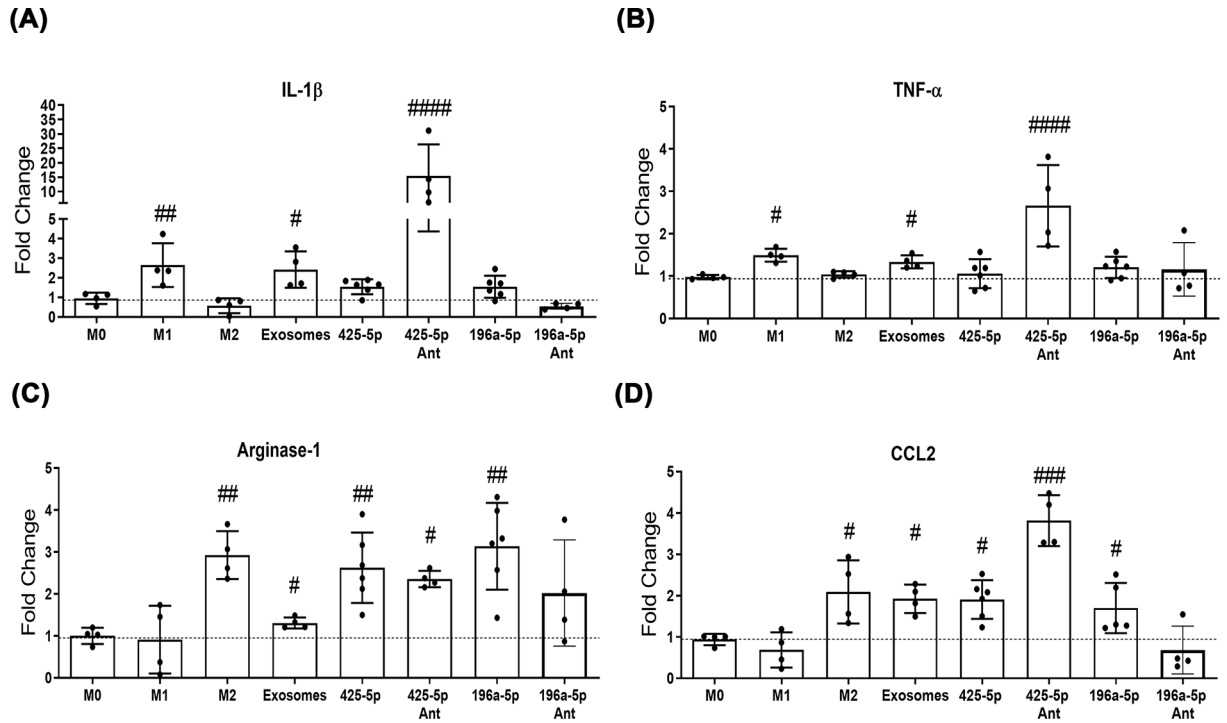

Figure 6. miR-196a-5p and miR-425-5p drive macrophage to alternative M2 immunophenotype

Macrophages were subjected to treatment with exosomes, miR-196a-5p or miR-425-5p mimics and antagomirs for 48 h, and gene expression of specific M1 and M2 immunophenotypes markers were evaluated qRT-PCR. Positive controls for M1 and M2 phenotypes were generated by treating macrophages with IFN-γ and IL-4, respectively. The bar graphs represent gene expression levels of IL-1β (**A**), TNF-α (**B**), arginase-1 (**C**), and CCL2 (**D**) in treated cells relative to control, data are presented as mean $\pm$ SD; at least four independent experiments. Graphs are presented as mean $\pm$ standard deviation. Statistical analysis was performed using a one-way analysis of variance followed by the Tukey test for multiple comparisons. $^{\#}P<0.05$, $^{\#\#}P<0.01$, $^{\#\#\#}P<0.001$, and $^{\#\#\#\#}P<0.0001$, relative to the control group.

myofibroblasts (Figure 7G–I), and these effects were not demonstrated in cells treated with miR-196a-5p antagomir (Figure 7H,I). The miR-425-5p mimic reduced Col I expression without affecting α-SMA levels and miR425-5p inhibition had no effects on myofibroblasts (Figure 7G–I). These findings suggest that rASC-derived exosomes and miR-196a-5p prevent and reverse TGF-β1 in infarct-induced myofibroblast differentiation, whereas exosomes and both miRNAs decreases collagen expression.

Discussion

We wanted to provide insights on the role of miRNAs in multicellular cardiac repair responses occurring post-MI. We profiled representative miRNAs from rACS-derived exosomes (candidates that influence processes in multiple cells) and identified miR-196a-5p and miR-425-5p not yet associated with the cardiac repair processes. These molecules recapitulated many critical cellular processes in a multicellular landscape with the potential to improve cardiac repair.

Cardiomyocyte proliferation is required for cardiac regeneration, currently a daunting goal for adult CMs. Under hypoxic conditions, neonatal CMs (which are more plastic cells) exhibited exosome-induced proliferation. Similarly, moderate hypoxia evoked neonatal CMs proliferation [40], and one of the pathways associated with this response is the hypoxia-inducible factor-1α (HIF-1α) stress pathway [41]. Exposure to rASC-derived exosomes through exosomal miR-31 modulates the factor-inhibiting hypoxia-inducible factor-1 (FIH1)/HIF-1α pathway and alleviates MI's effects by up-regulating endothelial cell proliferation and promoting enhanced blood perfusion [42]. In addition, other exosome-derived miRNAs promote the proliferation of CMs (e.g., miR-199a-5p), which has shown regenerative and reparative effects in MI models [23,43], although its clinical safety is a matter of concern [43].

Cell balance must be restored after ischemic events for cardiac repair to take place effectively. Exposure to miR-196a-5p and miR-425-5p mimics demonstrated protective effects in CMs, especially in hypoxic environments, although proliferation was not detected, confirming the repair and lack of regenerative potential of these miRNAs.

Clinical Science (2022) **136** 1281–1301
https://doi.org/10.1042/CS20220216

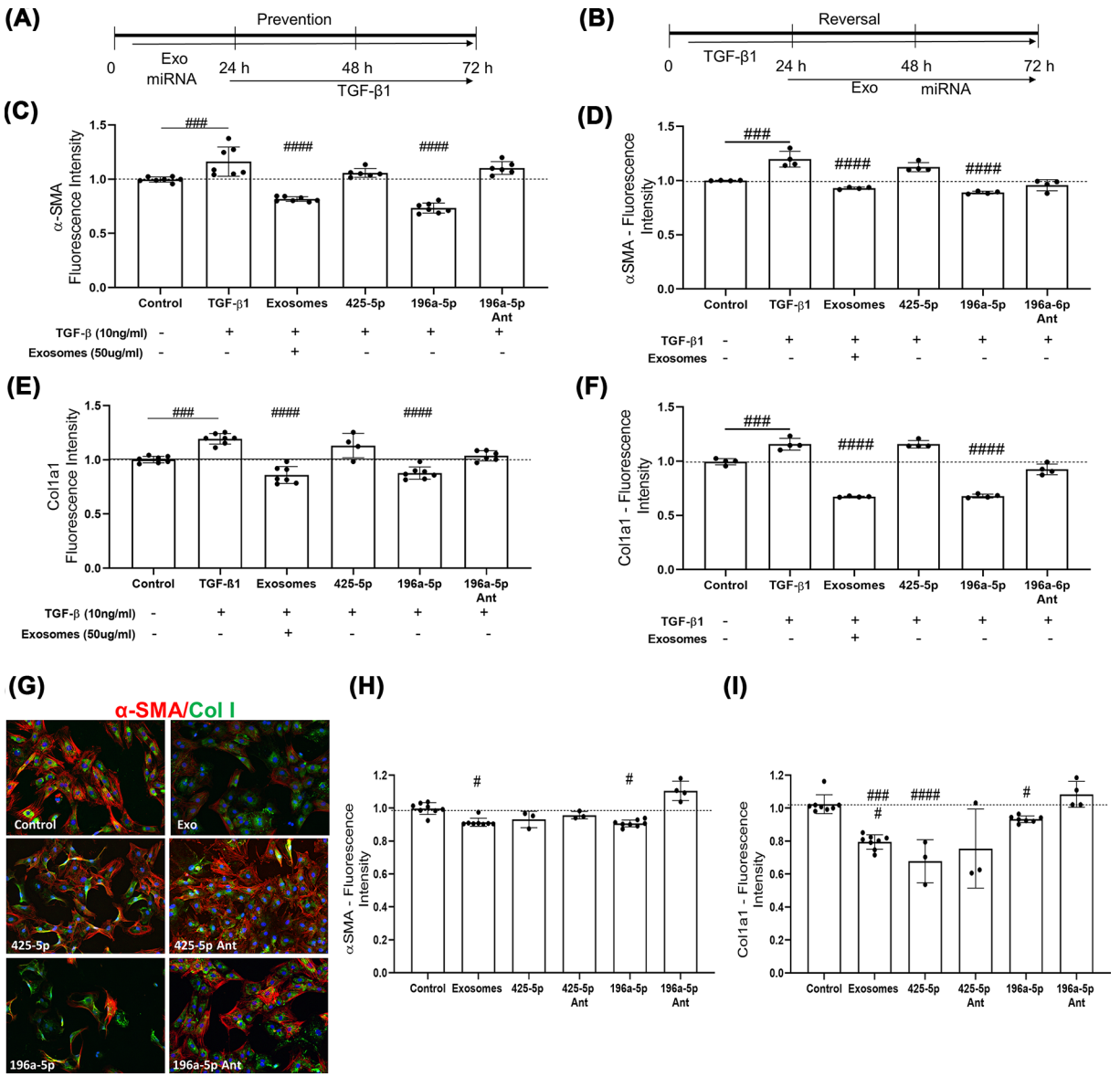

Figure 7. miR-196a-5p and miR-425-5p reduces fibroblast/myofibroblast profibrotic response

(**A**) Schematics of *in vitro* model to evaluate prevention potential of cardiac fibroblast activation by exosomes/miRNA. Cells were exposed to exosomes/miRNAs for 24 h and then to TGF-β1 for 72 h. (**B**) Schematics of *in vitro* model to evaluate reversal potential of cardiac fibroblast activation by exosomes/miRNA. Cells were exposed to TGF-β1 for 24 h and then to exosomes/miRNA for 72 h. Fibroblast activation was evaluated by immunofluorescence of α-SMA and Coll I proteins. The bar graphs represent the fold-change of α-SMA (**C,D**) and Coll I (**E,F**) mean fluorescence intensity in treated cells relative to control. (**G**) Representative micrograph of α-SMA/Coll I immunofluorescence in myofibroblasts isolated from rat infarcted hearts and treated with exosomes/miRNAs. The bar graphs represent the fold-change of α-SMA (**H**) and Coll I (**I**) mean fluorescence intensity in treated cells relative to control. Graphs are presented as mean ± standard deviation from at least three independent experiments. Statistical analysis was performed using a one-way analysis of variance followed by the Tukey test for multiple comparisons. $^{\#}P<0.05$, $^{\#\#}P<0.01$, $^{\#\#\#}P<0.001$ and $^{\#\#\#\#}P<0.0001$, relative to the control group.

These effects are complex and may be associated with improvements in mitochondrial homeostasis and dynamics. Decreased ROS generation associated with lactate production leads to improved mitochondrial integrity, reducing hypoxia-induced apoptotic signaling critical to propagate apoptosis by leaking mitochondrial cytochrome c and caspase activation [44,45].

Mitochondrial fusion protects against post-ischemia events and prevents CM death [46,47]. We observed that both miRNAs elevated mitofusin 1/2 levels (suggesting mitochondrial fusion) and miR-196a-5p increased mitochondria number with no changes in PGC1α protein levels.

In addition to the effects of miRNA-196a-5p in mitochondrial fusion, we speculate that alongside mitofusin 1/2, other genes that control mitochondrial membrane fusion, such as sirtuin 5 (SIRT5) and optic atrophy protein 1 (OPA-1), may also be modulated. SIRT5 is predicted to interact with miR-196 and, when elevated, promotes outer mitochondrial membrane fusion and improves healthy mitochondrial status in a hypoxic environment in CMs [48]. SIRT5 also controls PGC1α activation and tightly regulates fusion and mitochondrial biogenesis signaling [49]. OPA-1 is an inner mitochondrial membrane fusion protein predicted to interact with miR-196a-5p and is reduced during cardiac ischemia. Its overexpression improves mitochondrial homeostasis through increased mitochondrial fusion, improved cytochrome c distribution, and reduced levels of apoptosis [44,50]. Further studies are needed to test whether miRNA-196a-5p modulates SIRT5 and OPA-1 genes.

The effect of miR-425-5p on mitochondrial homeostasis and fusion is indirect and depends on the availability of the secondary messenger, inositol-1,4,5-triphosphate (IP_3). For ATP generation, IP_3 is required in inositol channel receptors (IP3Rs) that transport Ca^{2+} to the mitochondria [51]. The inositol polyphosphate-4-phosphatase type IA (INPP4A) gene catalyzes the transformation of phosphatidylinositol 3,4-bisphosphate ($PI_{(3,4)}P_2$) to IP_3, and its transcript contains sites of interaction with miR-425-5p. Thus, the reduced expression of the INPP4A gene may be one of the limiting factors in the generation of ATP and reduction of mitochondrial metabolism in CMs cultured in hypoxic conditions. In this context, increased mitochondrial fusion compensates to facilitate calcium transport between the sarcoplasmic reticulum (SR) and mitochondria, improving ATP generation. Mitofusin 2 is essential for exchanging ions between SR/mitochondria in a process mediated by the IP3R channel [52]. In addition, the inositol-triphosphate 3-kinase B gene, responsible for the phosphorylation of IP3 to Ins(1,3,4,5)P4 (IP_4), also contains regions of interaction with miR-425-5p. The IP_4 molecule competes with NADH substrates inhibiting the function of NOX family proteins [53]. Thus, a decrease in IPTKB gene expression by miR-425-5p may be associated with reduced ROS generation in CMs.

Angiogenesis is critical for the healing response and to restore myocardial blood flow post-MI, and there is a substantial body of evidence indicating that MSC-derived exosomes and miRNAs stimulate angiogenesis in animal models and endothelial cell cultures [24,54,55]. Our findings confirm these observations and demonstrate that miR-196a-5p and miR-425-5p recapitulate the exosome-induced increases in tube formation in HMVEC. Interestingly, miR-196a-5p showed a more consistent pattern and increased the proliferation rates in HCAEC and HMVEC, whereas exosomes and miR-425-5p's effects depended on the vascular bed origin. Indeed, Spred1, SEPT7, and PDGFRA genes associated with angiogenesis are targeted by miR-196a-5p and miR-425-5p [24,54,56]. Therefore, it is plausible that these miRNAs modulate the expression of genes critical for the signaling pathways controlling angiogenesis.

Resident macrophages under the post-injury immune response modulate different phases of tissue repair [57]. In myocardial infarction models, M2 macrophages improve cardiac function by reducing the release of proinflammatory cytokines [58]. RASC-derived exosomes promote M2 polarization by activating S1P/SK1/S1PR1 signaling [59]. We found that M0 macrophages exposed to exosomes polarize to M1 and M2 immunophenotypes. This finding highlights macrophages' plasticity in responding to exosomes; however, the finding also highlights the complex interplay among the diverse biomolecules in exosomes. By contrast, exposure to miR-196a-5p and miR-425-5p directed the cells only toward the M2 macrophage phenotype. In this regard, our bioinformatics analysis showed that miR-196a-5p targets genes associated with the IFN-γ response. The IFN-γ pathway is usually associated with macrophage M1 polarization; thus, a miR-196a-5p-induced down-regulation of INF-γ-related genes may reduce cytokine release and favor the alternative phenotype. For miR-425-5p, the bioinformatic analysis revealed the target activin A receptor type 1B, which belongs to the TGF-β superfamily. Activin A promotes M1 and inhibits M2 anti-inflammatory phenotypes [60]; therefore, overexpressing miR-425-5p in M0 macrophages might hamper the activin A receptor and favor the alternative anti-inflammatory markers and phenotype.

CFs play significant roles in tissue repair post-MI injuries because they prevent wall rupture; however, in excess, they might compromise cardiac function, which may progress to heart failure. We observed that exposure to exosomes was consistent with preventing fibroblast activation, reversing the number of αSMA+ activated myofibroblasts, and decreasing collagen synthesis associated with a fibrogenic stimulus. RASC-derived exosomes exposure reduces fibroblast differentiation to myofibroblasts induced by rigid matrixes, similar to those found in fibrotic tissue, by reducing angiotensin II type 1 receptor and up-regulation of SMAD7 [61]. MiR-196a-5p reproduced all exosome effects in fibroblasts, which may be related to genes responsible for fibrogenic responses, such as the TGFβ receptor III, SMAD-binding elements, and collagen synthesis genes. Moreover, miR-196a-5p reduces the progression of fibrosis

Clinical Science (2022) **136** 1281–1301
https://doi.org/10.1042/CS20220216

in renal ischemia–reperfusion models through a sponging effect of the long non-coding RNA H19 associated with the regulation of the Wnt1/β-catenin pathway [62]. MiR-196a-5p also regulates the SMAD6 gene and the proliferation of gastric cancer cells; however, this effect depends on the endogenous competition with lncFGD5-AS1 [63]. Thus, there are several ways whereby mir-196a-5p may modulate the progression of fibrosis and cell proliferation. As for miR-425-5p, we observed a reduction in collagen production only in rats' myofibroblasts derived from infarcted tissue. This response may be associated with the high energy demand required for collagen assembly and deposition, and miR-425-5p (as previously discussed) contains putative interaction sites with genes that regulate the energetic cascade, such as in the inositol triphosphate and MAPK pathways.

We have provided evidence that increased or decreased expression of miRs 196a-5p and 425-5p modulate cellular events related to cardiac repair, even though in complex systems this binary notion may be too simplistic. Manipulating the miRNA individual content within the exosomes *in vitro* is an elegant approach to further confirm our observations, although very challenging. Moreover, the successful use of mimics and inhibitors depend on the levels of constitutive gene expression and availability of miRNAs within a cellular context that is poorly characterized. Thus, most of our observations took advantage of the fact that the two miRNAs were down-regulated by myocardium infarction and therefore, we could at least increase their levels to assess downstream processes that influence cardiac repair. Extreme modulation of miRNA levels is unlikely to happen *in vivo*; hence further studies are needed to demonstrate the physiological relevance of these miRNAs in cardiac repair.

In summary, we provided evidence that miR-196a-5p and miR-425-5p affect several cells and phenotypes that potentially improve cardiac repair post-MI. The mechanisms associated with the beneficial effects of each of the miRNAs are consistent with their specific genes and pathways. MiR-196a-5p targets genes of mitochondrial fusion pathways, endothelial proliferation, and fibroblast activation, whereas the beneficial effects of miR-425-5p may be related to its broad influence on energetic pathways genes.

Clinical perspectives

- Adipose stem cell cardiac transplantation improves the post-myocardial infarction response associated with the paracrine effects of biomolecules resulting from transient cell engraftment. Candidate biomolecules include miRNAs secreted or shuttled out of cells in exosomes, contributing to the improved cardiac repair response. Little is known about the effects of exosome miRNAs on cardiac target cells that may minimize the effects of myocardial infarction.

- We identified miR-196a-5p and miR-425-5p, two miRNAs that had not been explored in the cardiac repair response and are down-regulated by myocardial infarction. Both miRNAs protected the viability and reactive oxygen species production in cardiomyocytes in a hypoxic environment, increased tube formation by endothelial cells, and drove macrophages to an anti-inflammatory M2 immunophenotype. Moreover, miR-196a-5p reduced and reversed fibroblast activation and decreased collagen expression, which are critical antifibrotic properties.

- These miRNAs have the potential to direct therapeutic approaches that minimize cardiac injury post-myocardial infarction to improve outcomes.

Data Availability

Data presented in this manuscript are available from the corresponding authors upon reasonable request.

Competing Interests

The authors declare that there are no competing interests associated with the manuscript.

Funding

This work was supported by the Fundação de Amparo à Pesquisa do Estado de São Paulo (FAPESP) [grant numbers 2013/17368-0 (to J.E.K.), 15/50216-5 (to J.E.K.), 2017/07024-3 (to C.Z.), 2017/17296-0 (to N.C.O.)]; and the Conselho Nacional de Pesquisa (CNPq) [INCT - 465586/2014-7, 309179/2013-0 and 441020/2018-6 (to J.E.K.)].

CRediT Author Contribution

Nathalia C. de Almeida Oliveira: Conceptualization, Data curation, Formal analysis, Investigation, Methodology, Writing—original draft. **Elida A. Neri:** Formal analysis, Validation, Investigation, Visualization, Writing—original draft, Writing—review & editing. **Caio M. Silva:** Formal analysis, Validation, Investigation, Visualization, Methodology, Writing—original draft, Writing—review & editing. **Iuri C. Valadão:** Validation, Investigation, Methodology, Writing—review & editing. **Miriam H. Fonseca-Alaniz:** Investigation, Visualization, Methodology. **Camila Zogbi:** Investigation, Visualization, Methodology. **Débora Levy:** Investigation, Methodology. **Sergio P. Bydlowski:** Investigation, Methodology. **Jose Eduardo Krieger:** Conceptualization, Resources, Supervision, Funding acquisition, Project administration, Writing—review & editing.

Acknowledgements

We thank Dr. Mariliza Rodrigues and Mariana L. P. de Carvalho for their assistance with the validation of the gene expression assays and qPCR analysis. We also thank Fundação de Amparo a Pesquisa do Estado de São Paulo (FAPESP) and Conselho Nacional de Pesquisa (CNPq) for the funding support. This study was financed in part by the Coordenação de Aperfeiçoamento de Pessoal de Nível Superior - Brasil (CAPES 88887.643917/2021-00).

Abbreviations

ASC, adipose-derived stem cells; CM, cardiomyocyte; HIF-1α, hypoxia-inducible factor-1α; OPA-1, optic atrophy protein 1; RCMVEC, rat cardiac microvascular endothelial cell; SIRT5, sirtuin 5; SR, sarcoplasmic reticulum.

References

1 Porrello, E.R., Mahmoud, A.I., Simpson, E., Hill, J.A., Richardson, J.A., Olson, E.N. et al. (2011) Transient regenerative potential of the neonatal mouse heart. *Science* **331**, 1078–1080, https://doi.org/10.1126/science.1200708
2 Zogbi, C., Saturi de Carvalho, A.E.T., Nakamuta, J.S., de M. Caceres, V., Prando, S. et al. (2014) Early postnatal rat ventricle resection leads to long-term preserved cardiac function despite tissue hypoperfusion. *Physiol. Rep.* **2**, e12115, https://doi.org/10.14814/phy2.12115
3 Wang, Z., Cui, M., Shah, A.M., Ye, W., Tan, W., Min, Y.L. et al. (2019) Mechanistic basis of neonatal heart regeneration revealed by transcriptome and histone modification profiling. *Proc. Natl. Acad. Sci. U.S.A.* **116**, 18455–18465, https://doi.org/10.1073/pnas.1905824116
4 Dariolli, R., Naghetini, M.V., Marques, E.F., Takimura, C.K., Jensen, L.S., Kiers, B. et al. (2017) Allogeneic pASC transplantation in humanized pigs attenuates cardiac remodeling post-myocardial infarction. *PLoS ONE* **12**, e0176412, https://doi.org/10.1371/journal.pone.0176412
5 Burnett, H., Earley, A., Voors, A.A., Senni, M., McMurray, J.J.V., Deschaseaux, C. et al. (2017) Thirty years of evidence on the efficacy of drug treatments for chronic heart failure with reduced ejection fraction: a network meta-analysis. *Circ. Heart Fail.* **10**, https://doi.org/10.1161/CIRCHEARTFAILURE.116.003529
6 Frangogiannis, N.G. (2012) Matricellular proteins in cardiac adaptation and disease. *Physiol. Rev.* **92**, 635–688, https://doi.org/10.1152/physrev.00008.2011
7 Frangogiannis, N.G. (2015) Pathophysiology of myocardial infarction. *Compr. Physiol.* **5**, 1841–1875, https://doi.org/10.1002/cphy.c150006
8 Frangogiannis, N.G. (2014) The inflammatory response in myocardial injury, repair, and remodelling. *Nat. Rev. Cardiol.* **11**, 255–265, https://doi.org/10.1038/nrcardio.2014.28
9 Ma, Y., De Castro Brás, L.E., Toba, H., Iyer, R.P., Hall, M.E., Winniford, M.D. et al. (2014) Myofibroblasts and the extracellular matrix network in post-myocardial infarction cardiac remodeling. *Pflugers Arch.* **466**, 1113–1127, https://doi.org/10.1007/s00424-014-1463-9
10 Xin, M., Olson, E.N. and Bassel-Duby, R. (2013) Mending broken hearts: cardiac development as a basis for adult heart regeneration and repair. *Nat. Rev. Mol. Cell Biol.* **14**, 529–541, https://doi.org/10.1038/nrm3619
11 Cai, L., Johnstone, B.H., Cook, T.G., Tan, J., Fishbein, M.C., Chen, P.-S. et al. (2009) IFATS collection: Human adipose tissue-derived stem cells induce angiogenesis and nerve sprouting following myocardial infarction, in conjunction with potent preservation of cardiac function. *Stem Cells* **27**, 230–237, https://doi.org/10.1634/stemcells.2008-0273
12 Dai, W., Hale, S.L. and Kloner, R.A. (2007) Role of a paracrine action of mesenchymal stem cells in the improvement of left ventricular function after coronary artery occlusion in rats. *Regen. Med.* **2**, 63–68, https://doi.org/10.2217/17460751.2.1.63
13 Danieli, P., Malpasso, G., Ciuffreda, M.C. and Gnecchi, M. (2016) Testing the paracrine properties of human mesenchymal stem cells using conditioned medium. *Methods Mol. Biol.* **1416**, 445–456, https://doi.org/10.1007/978-1-4939-3584-0˙26
14 Gallina, C., Turinetto, V. and Giachino, C. (2015) A new paradigm in cardiac regeneration: the mesenchymal stem cell secretome. *Stem Cells Int.* **2015**, 765846, https://doi.org/10.1155/2015/765846
15 Gnecchi, M., Danieli, P., Malpasso, G. and Ciuffreda, M.C. (2016) Paracrine mechanisms of mesenchymal stem cells in tissue repair. *Methods Mol. Biol.* **1416**, 123–146, https://doi.org/10.1007/978-1-4939-3584-0˙7
16 Gnecchi, M., He, H., Liang, O.D., Melo, L.G., Morello, F., Mu, H. et al. (2005) Paracrine action accounts for marked protection of ischemic heart by Akt-modified mesenchymal stem cells. *Nat. Med.* **11**, 367–368, https://doi.org/10.1038/nm0405-367
17 Leiker, M., Suzuki, G., Iyer, V.S., Canty, J.M. and Lee, T. (2008) Assessment of a nuclear affinity labeling method for tracking implanted mesenchymal stem cells. *Cell Transplant.* **17**, 911–922, https://doi.org/10.3727/096368908786576444
18 Danoviz, M.E., Nakamuta, J.S., Marques, F.L.N., dos Santos, L., Alvarenga, E.C., dos Santos, A.A. et al. (2010) Rat adipose tissue-derived stem cells transplantation attenuates cardiac dysfunction post infarction and biopolymers enhance cell retention. *PLoS ONE* **5**, https://doi.org/10.1371/journal.pone.0012077

Clinical Science (2022) **136** 1281–1301
https://doi.org/10.1042/CS20220216

19 Colombo, M., Raposo, G. and Théry, C. (2014) Biogenesis, secretion, and intercellular interactions of exosomes and other extracellular vesicles. *Annu. Rev. Cell Dev. Biol.* **30**, 255–289, https://doi.org/10.1146/annurev-cellbio-101512-122326
20 Valadi, H., Ekström, K., Bossios, A., Sjöstrand, M., Lee, J.J. and Lötvall, J.O. (2007) Exosome-mediated transfer of mRNAs and microRNAs is a novel mechanism of genetic exchange between cells. *Nat. Cell Biol.* **9**, 654–659, https://doi.org/10.1038/ncb1596
21 Van Niel, G., D'Angelo, G. and Raposo, G. (2018) Shedding light on the cell biology of extracellular vesicles. *Nat. Rev. Mol. Cell Biol.* **19**, 213–228, https://doi.org/10.1038/nrm.2017.125
22 Garcia-Martin, R., Wang, G., Brandão, B.B., Zanotto, T.M., Shah, S., Kumar Patel, S. et al. (2022) MicroRNA sequence codes for small extracellular vesicle release and cellular retention. *Nature* **601**, 446–451, https://doi.org/10.1038/s41586-021-04234-3
23 Eulalio, A., Mano, M., Ferro, M.D., Zentilin, L., Sinagra, G., Zacchigna, S. et al. (2012) Functional screening identifies miRNAs inducing cardiac regeneration. *Nature* **492**, 376–381, https://doi.org/10.1038/nature11739
24 Ferguson, S.W., Wang, J., Lee, C.J., Liu, M., Neelamegham, S., Canty, J.M. et al. (2018) The microRNA regulatory landscape of MSC-derived exosomes: a systems view. *Sci. Rep.* **8**, 1–12, https://doi.org/10.1038/s41598-018-19581-x
25 Verjans, R., Derks, W.J.A., Korn, K., Sönnichsen, B., van Leeuwen, R.E.W., Schroen, B. et al. (2019) Functional screening identifies MicroRNAs as multi-cellular regulators of heart failure. *Sci. Rep.* **9**, 1–15, https://doi.org/10.1038/s41598-019-41491-9
26 Song, Y., Zhang, C., Zhang, J., Jiao, Z., Dong, N., Wang, G. et al. (2019) Localized injection of miRNA-21-enriched extracellular vesicles effectively restores cardiac function after myocardial infarction. *Theranostics* **9**, 2346–2360, https://doi.org/10.7150/thno.29945
27 Peoples, J.N., Saraf, A., Ghazal, N., Pham, T.T. and Kwong, J.Q. (2019) Mitochondrial dysfunction and oxidative stress in heart disease. *Exp. Mol. Med.* **51**, 1–13, https://doi.org/10.1038/s12276-019-0355-7
28 Théry, C., Amigorena, S., Raposo, G. and Clayton, A. (2006) Isolation and characterization of exosomes from cell culture supernatants and biological fluids. *Curr. Protoc. Cell Biol.*, Chapter 3 3.22.1- 3.22.29, https://doi.org/10.1002/0471143030.cb0322s30
29 Liang, X., Zhang, L., Wang, S., Han, Q. and Zhao, R.C. (2016) Exosomes secreted by mesenchymal stem cells promote endothelial cell angiogenesis by transferring miR-125a. *J. Cell Sci.* **129**, 2182–2189, https://doi.org/10.1242/jcs.170373
30 Schindelin, J., Arganda-Carreras, I., Frise, E., Kaynig, V., Longair, M., Pietzsch, T. et al. (2012) Fiji: an open-source platform for biological-image analysis. *Nat. Methods* **9**, 676–682, https://doi.org/10.1038/nmeth.2019
31 Zhou, X.L., Fang, Y.-H., Wan, L., Xu, Q.-R., Huang, H., Zhu, R.-R. et al. (2019) Notch signaling inhibits cardiac fibroblast to myofibroblast transformation by antagonizing TGF-β1/Smad3 signaling. *J. Cell. Physiol.* **234**, 8834–8845, https://doi.org/10.1002/jcp.27543
32 Jensen, L., Neri, E., Bassaneze, V., De Almeida Oliveira, N.C., Dariolli, R., Turaça, L.T. et al. (2018) Integrated molecular, biochemical, and physiological assessment unravels key extraction method mediated influences on rat neonatal cardiomyocytes. *J. Cell. Physiol.* **233**, 5420–5430, https://doi.org/10.1002/jcp.26380
33 Carpenter, A.E., Jones, T.R., Lamprecht, M.R., Clarke, C., Kang, I.H., Friman, O. et al. (2006) CellProfiler: image analysis software for identifying and quantifying cell phenotypes. *Genome Biol.* **7**, https://doi.org/10.1186/gb-2006-7-10-r100
34 Riccardi, C. and Nicoletti, I. (2006) Analysis of apoptosis by propidium iodide staining and flow cytometry. *Nat. Protoc.* **1**, 1458–1461, https://doi.org/10.1038/nprot.2006.238
35 Livak, K.J. and Schmittgen, T.D. (2001) Analysis of relative gene expression data using real-time quantitative PCR and the 2(-Delta Delta C(T)) Method. *Methods* **25**, 402–408, https://doi.org/10.1006/meth.2001.1262
36 Ru, Y., Kechris, K.J., Tabakoff, B., Hoffman, P., Radcliffe, R.A., Bowler, R. et al. (2014) The multiMiR R package and database: integration of microRNA-target interactions along with their disease and drug associations. *Nucleic Acids Res.* **42**, e133, https://doi.org/10.1093/nar/gku631
37 Csárdi, G. and Nepusz, T. The igraph software package for complex network research.
38 Wu, T., Hu, E., Xu, S., Chen, M., Guo, P., Dai, Z. et al. (2021) clusterProfiler 4.0: a universal enrichment tool for interpreting omics data. *Innov. (New York, NY)* **2**, 100141, https://doi.org/10.1016/j.xinn.2021.100141
39 Huang, D.W., Sherman, B.T. and Lempicki, R.A. (2009) Systematic and integrative analysis of large gene lists using DAVID bioinformatics resources. *Nat. Protoc.* **4**, 44–57, https://doi.org/10.1038/nprot.2008.211
40 Nakada, Y., Canseco, D.C., Thet, S., Abdisalaam, S., Asaithamby, A., Santos, C.X. et al. (2017) Hypoxia induces heart regeneration in adult mice. *Nature* **541**, 222–227, https://doi.org/10.1038/nature20173
41 Guimarães-Camboa, N., Stowe, J., Aneas, I., Sakabe, N., Cattaneo, P., Henderson, L. et al. (2015) HIF1α represses cell stress pathways to allow proliferation of hypoxic fetal cardiomyocytes. *Dev. Cell* **33**, 507–521, https://doi.org/10.1016/j.devcel.2015.04.021
42 Zhu, D., Wang, Y., Thomas, M., McLaughlin, K.A., Oguljahan, B., Henderson, J. et al. (2022) Exosomes from adipose-derived stem cells alleviate myocardial infarction via microRNA-31/FIH1/HIF-1α pathway. *J. Mol. Cell Cardiol.* **162**, 10–19, https://doi.org/10.1016/j.yjmcc.2021.08.010
43 Gabisonia, K., Prosdocimo, G., Aquaro, G.D., Carlucci, L., Zentilin, L., Secco, I. et al. (2019) MicroRNA therapy stimulates uncontrolled cardiac repair after myocardial infarction in pigs. *Nature* **569**, 418–422, https://doi.org/10.1038/s41586-019-1191-6
44 Xin, T., Lv, W., Liu, D., Jing, Y. and Hu, F. (2020) Opa1 reduces hypoxia-induced cardiomyocyte death by improving mitochondrial quality control. *Front. Cell Dev. Biol.* **8**, 853, https://doi.org/10.3389/fcell.2020.00853
45 Zhou, H., Hu, S., Jin, Q., Shi, C., Zhang, Y., Zhu, P. et al. (2017) Mff-dependent mitochondrial fission contributes to the pathogenesis of cardiac microvasculature ischemia/reperfusion injury via induction of mROS-mediated cardiolipin oxidation and HK2/VDAC1 disassociation-involved mPTP opening. *J. Am. Heart Assoc.* **6**, https://doi.org/10.1161/JAHA.116.005328
46 Zhang, Y., Wang, Y., Xu, J., Tian, F., Hu, S., Chen, Y. et al. (2019) Melatonin attenuates myocardial ischemia-reperfusion injury via improving mitochondrial fusion/mitophagy and activating the AMPK-OPA1 signaling pathways. *J. Pineal Res.* **66**, https://doi.org/10.1111/jpi.12542
47 Ong, S.B., Subrayan, S., Lim, S.Y., Yellon, D.M., Davidson, S.M. and Hausenloy, D.J. (2010) Inhibiting mitochondrial fission protects the heart against ischemia/reperfusion injury. *Circulation* **121**, 2012–22, https://doi.org/10.1161/CIRCULATIONAHA.109.906610

48 Liu, B., Che, W., Zheng, C., Liu, W., Wen, J., Fu, H. et al. (2013) SIRT5: a safeguard against oxidative stress-induced apoptosis in cardiomyocytes. *Cell. Physiol. Biochem.* **32**, 1050–59, https://doi.org/10.1159/000354505
49 Buler, M., Aatsinki, S.M., Izzi, V., Uusimaa, J. and Hakkola, J. (2014) SIRT5 is under the control of PGC-1α and AMPK and is involved in regulation of mitochondrial energy metabolism. *FASEB J.* **28**, 3225–3237, https://doi.org/10.1096/fj.13-245241
50 Xin, T. and Lu, C. (2020) Irisin activates Opa1-induced mitophagy to protect cardiomyocytes against apoptosis following myocardial infarction. *Aging (Albany NY)* **12**, 4474–4488, https://doi.org/10.18632/aging.102899
51 Suman, M., Sharpe, J.A., Bentham, R.B., Kotiadis, V.N., Menegollo, M., Pignataro, V. et al. (2018) Inositol trisphosphate receptor-mediated Ca2+ signalling stimulates mitochondrial function and gene expression in core myopathy patients. *Hum. Mol. Genet.* **27**, 2367–2382, https://doi.org/10.1093/hmg/ddy149
52 Seidlmayer, L.K., Mages, C., Berbner, A., Eder-Negrin, P., Arias-Loza, P.A., Kaspar, M. et al. (2019) Mitofusin 2 is essential for IP 3-mediated SR/mitochondria metabolic feedback in ventricular myocytes. *Front. Physiol.* **10**, https://doi.org/10.3389/fphys.2019.00733
53 Li, J., Zheng, C., Wang, M., Umano, A.D., Dai, Q., Zhang, C. et al. (2022) ROS-regulated phosphorylation of ITPKB by CAMK2G drives cisplatin resistance in ovarian cancer. *Oncogene* **41**, 1114–1128, https://doi.org/10.1038/s41388-021-02149-x
54 Liu, B., Wang, B., Zhang, X., Lock, R., Nash, T. and Vunjak-Novakovic, G. (2021) Cell type-specific microRNA therapies for myocardial infarction. *Sci. Transl. Med.* **13**, eabd0914, https://doi.org/10.1126/scitranslmed.abd0914
55 Ma, T., Chen, Y., Chen, Y., Meng, Q., Sun, J., Shao, L. et al. (2018) MicroRNA-132, delivered by mesenchymal stem cell-derived exosomes, promote angiogenesis in myocardial infarction. *Stem Cells Int.* **2018**, https://doi.org/10.1155/2018/3290372
56 McGeary, S.E., Lin, K.S., Shi, C.Y., Pham, T.M., Bisaria, N., Kelley, G.M. et al. (2019) The biochemical basis of microRNA targeting efficacy. *Science (80-)* **366**, eaav1741, https://doi.org/10.1126/science.aav1741
57 Revelo, X.S., Parthiban, P., Chen, C., Barrow, F., Fredrickson, G., Wang, H. et al. (2021) Cardiac resident macrophages prevent fibrosis and stimulate angiogenesis. *Circ. Res.* **129**, 1086–1101, https://doi.org/10.1161/CIRCRESAHA.121.319737
58 Gao, Y., Qian, N., Xu, J. and Wang, Y. (2021) The roles of macrophages in heart regeneration and repair after injury. *Front. Cardiovasc. Med.* **8**, 1–10, https://doi.org/10.3389/fcvm.2021.744615
59 Deng, S., Zhou, X., Ge, Z., Song, Y., Wang, H., Liu, X. et al. (2019) Exosomes from adipose-derived mesenchymal stem cells ameliorate cardiac damage after myocardial infarction by activating S1P/SK1/S1PR1 signaling and promoting macrophage M2 polarization. *Int. J. Biochem. Cell Biol.* **114**, https://doi.org/10.1016/j.biocel.2019.105564
60 Sierra-Filardi, E., Puig-Kröger, A., Blanco, F.J., Nieto, C., Bragado, R., Palomero, M.I. et al. (2011) Activin A skews macrophage polarization by promoting a proinflammatory phenotype and inhibiting the acquisition of anti-inflammatory macrophage markers. *Blood* **117**, 5092–5101, https://doi.org/10.1182/blood-2010-09-306993
61 Yong, K.W., Li, Y., Liu, F., Gao, B., Lu, T.J., Wan Abas, W.A.B. et al. (2016) Paracrine effects of adipose-derived stem cells on matrix stiffness-induced cardiac myofibroblast differentiation via angiotensin II type 1 receptor and Smad7. *Sci. Rep.* **6**, https://doi.org/10.1038/srep33067
62 Dong, X., Cao, R., Li, Q. and Yin, L. (2022) The long noncoding RNA-H19 mediates the progression of fibrosis from acute kidney injury to chronic kidney disease by regulating the miR-196a/Wnt/β-catenin signaling. *Nephron* **146**, 209–219, https://doi.org/10.1159/000518756
63 Liu, L., Zhang, C., Wang, J., Liu, X., Qu, H., Zhang, G. et al. (2021) A high level of lncFGD5-AS1 inhibits epithelial-to-mesenchymal transition by regulating the miR-196a-5p/SMAD6/BMP axis in gastric cancer. *BMC Cancer* **21**, https://doi.org/10.1186/s12885-021-08192-x